



MSc in Physics

Influence of pH on diphtheria anatoxin incorporation into SBA-15

Madalena Branco

Supervised by Heloisa Nunes Bordallo and Pedro Leonidas Oseliero Filho

August 2023



Abstract

Oral vaccines are preferred to intramuscular injections used today for diphtheria vaccine, due to ease of administration, non-invasiveness and convenience, since they are cheaper and require less technical skills. However, oral vaccines require the use of delivery vehicles for the passage through the gastrointestinal tract to protect the antigen from physiological barriers. To stimulate an immune response we need a specific amount of anatoxin, which needs to be incorporated into that carrier to get in contact with our immune system.

Previous studies have already reported on the efficiency of using SBA-15 as a nanocarrier for diphtheria. Nevertheless, finding optimal encapsulation conditions is essential to enable maximal protein uptake, while minimizing aggregation. Since the incorporation of DT into SBA-15 is performed in aqueous medium, the process is highly affected by electrostatic and hydrophilic interactions, therefore it is relevant to find the optimal environmental condition, considering pH, ionic strength and concentrations. The main goal of this project was to experimentally find the optimal pH and protein concentration for encapsulation.

To measure the protein uptake, we used UV-vis spectroscopy and thermal gravimetric analysis coupled to a Fourier transform infrared spectroscopy and mass spectrometry (TGA-FTIR-MS). The last technique is also used for chemical characterization of the samples.

From the analysis of diphtheria anatoxin incorporated into SBA-15, at different pHs and concentrations, we concluded that thermal degradation profiles and water dynamics are different, depending on pH, but overall all samples displayed a similar behaviour. We observed higher adsorption and earlier

protein degradation for lower pHs. We hypothesize that pH 2.9 is the best pH, since it allows for higher adsorption levels, but more experiments should be performed, in order to understand if it is the ideal pH for encapsulation.

Acknowledgements

I would like to start by thanking both of my supervisors, Heloisa Nunes Bordallo and Pedro Oseliero Filho, without them, this project would not have been possible. Thank you for your guidance and support throughout these 9 months. Thank you, Pedro, for your patience and attention to answer my questions and teach me how to work in the lab. Thank you, Heloisa, for the hours spent helping me interpret and correlate the endless amount of data. Finally, thank you, both for all the comments and constructive feedback you have been giving me and especially for helping me trust myself and my ideas.

I would like to thank all of the group members, that I had the pleasure to work with. For all of the discussions and new insights you gave me during groups meetings or private conversations. For the ones that I shared an office with, a special thank you for the companionship and good disposition you brought with you.

On a more personal level, I want to thank my friends, that allowed me to complain and laugh. A special thank you to Eva and Sofie, for cheering me up, when necessary and for all the good experiences we shared together and for Luna, for always being by my side, throughout this two years. Finally, the biggest thank you to my family for supporting me, financially, emotionally and in any imaginable way. I would not be who I am and where I am today, without you.

I am very thankful for everyone, mentioned or not, that positively contributed to my work and well being and grateful for having the opportunity to be a part of this project and learn as much as I did.

Contents

1	Introduction	1
2	Materials and Methods	9
2.1	Samples	9
2.2	Sample Preparation	10
2.3	Protein Adsorption Measurements	15
2.3.1	Basics of UV-Vis spectroscopy	16
2.3.2	Adsorption isotherm Fit	18
2.4	Thermal Analysis of samples	20
2.4.1	Basics of TGA-FTIR-MS	20
3	Results and Discussion	29
3.1	SBA-15 characterization	29
3.2	Lysozyme Results	32
3.2.1	Lys adsorption into SBA-15	32
3.2.2	Thermal Analysis of Lys samples	34
3.3	Characterization of Control Samples	38
3.4	DT results	42
3.4.1	DT adsorption into SBA-15	42
3.4.2	Thermal Analysis of DT samples	45
4	Conclusion	58
5	Perspectives	60
	Bibliography	62
6	Appendix	69
6.1	Appendix A	69
6.2	Appendix B	71
6.3	Appendix C	72
6.4	Appendix D	74

6.5	Appendix E	76
6.6	Appendix F	76
6.7	Appendix G	78

Introduction

Diphtheria is a highly transmittable bacterial infection caused by *Corynebacterium diphtheriae*, which produces a toxin that inhibits cellular protein synthesis and forms a characteristic pseudomembrane on infected tissue. The toxin is absorbed into the bloodstream and can affect different organs and tissues further away from the infection site [1]. Classical diphtheria affects the throat and nose. It can cause severe complication, such as pneumonia, lung failure, and ultimately death. It usually spreads through oral or respiratory droplets. Cutaneous diphtheria prevails over classic diphtheria in tropical and subtropical regions. It causes rashes and ulcers and can also spread from contact with infected skin [2].

Diphtheria was a major cause of disease and death in the nineteenth century. Nowadays it is treatable and rare due to mass vaccination. The basis of this vaccine is the diphtheria toxoid or anatoxin (DT) with a molecular weight of 58.3 kDa and a size of approximately 9.2 nm [3]. DT is a formaldehyde-inactivated diphtheria toxin [2]: when formaldehyde is mixed with protein, it results in the formation of inter- and intra-molecular bonds as methylene bridges. These bridges are able to change the proteins' properties, making it very stable and heat resistant [4]. Vaccination programs usually combine this vaccine with tetanus and/or pertussis vaccine. These vaccines are administered by intramuscular injection and contain aluminum hydroxide as an adjuvant [1]. Adjuvants work as an enhancer of the immune response[5].

Toxoid immunization has been very successful, but rare outbreaks in countries where the disease is endemic still occur. In 2022, 391 cases have been reported: 80 % of these cases were among newly arrived immigrants, such as refugees and asylum seekers, mostly from Afghanistan, but also from Albania, Algeria, Bangladesh, Cameroon, Iran, Iraq, Morocco, Pakistan, Russian Federation, Syria, Tunisia and Turkey [6]. Therefore, it is important to maintain mass vaccination, especially in developing countries, where poorly immunized groups exist [1]. The development of an oral vaccine for diphtheria would

solve this problem, since it is easier to administrate (non-invasive), which also makes it cheaper: less need for medical staff and materials, such as needles and syringes[1, 3, 7, 8].

However, approved oral vaccines for different diseases are not common due to the difficulty of their design - this route forces the vaccine to face many physiological barriers. It starts with the passage through the gastrointestinal tract (GI tract), where it has to travel from the mouth to the intestines, facing a harsh environment (change in pH along the tract and presence of digestive enzymes), which can lead to protein denaturation (unfolding of its structure and loss of function). This first barrier requires the use of a delivery system that protects the vaccine from the environment. Once it reaches the intestine, the vaccine needs to get in contact with M cells (located in the epithelium). M cells are part of the gut-associated lymphoid tissue (GALT) and are responsible for sampling and transporting the antigen from the intestine lumen to the underlying immune cells, such as B and T cells, located at the Peyer’s patches (PP). This step requires the targeting of specific cells, such as M cells, for example, and the release of the vaccine at the correct site (Fig. 1.1). T and B lymphocytes, are then responsible for creating an adaptive immune response [7, 9, 10].

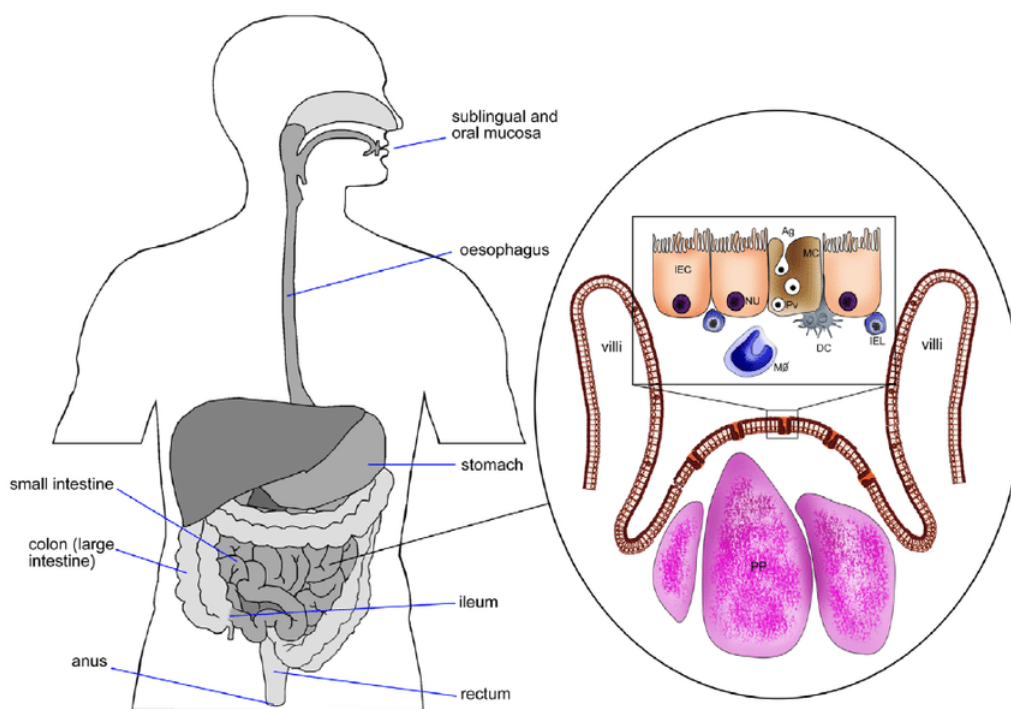


Figure 1.1: Scheme of of intestinal epithelium extracted from [10] showing MC (M cells), PP(Peyer’s patches) and the intestinal epithelial cells (IEC).

Usage of Santa Barbara Amorphous 15 (SBA-15), an ordered mesoporous silica (OMS), described in more details below, as a nanocarrier has been studied for different proteins and its potential use for oral vaccination has been showing promising results [11, 12, 13]. For diphtheria vaccine, Rasmussen et. al [3] have shown that, for a protein concentration of 0.5 mg/ml or lower, diluted in PBS buffer (pH = 7), SBA-15 did not affect DT's conformation after incorporation, has the ability to protect the vaccine from thermal degradation and pH variations and it even showed higher antibody titers, using SBA-15 as an adjuvant, than using the typical aluminum hydroxide. Therefore, it shows that SBA-15 can act as a nanocarrier, entrapping the antigen inside its mesopore, and as an adjuvant, increasing DT's efficiency in producing an immune response.

SBA-15 is formed by approximately 20 μm particles with hexagonal ordered pores with 4-12 nm of diameter (mesopores) and larger than 50 nm (macropores). Along the walls of the mesopores, there are pores with less than 2 nm of diameter (micropores) [14] - see Fig. 1.2. Fig. 1.3 shows a schematic representation of SBA-15 synthesis: it requires the use of surfactants to form micelles, typically tri-block copolymer, followed by addition of silica precursor and a heat treatment. During this step, there is a formation of a solid matrix, mainly constituted by siloxane (Si-O-Si), formed via condensation of silanol groups (Si-OH) [15] (Fig. 1.4). The polymer is removed by calcination, which leads to a silica structure with pores. The structure and pore size depends on the size and shape of the micelles [16, 17]. SBA-15's surface is composed by hydrophobic siloxane groups and hydrophilic silanol groups [15, 18].

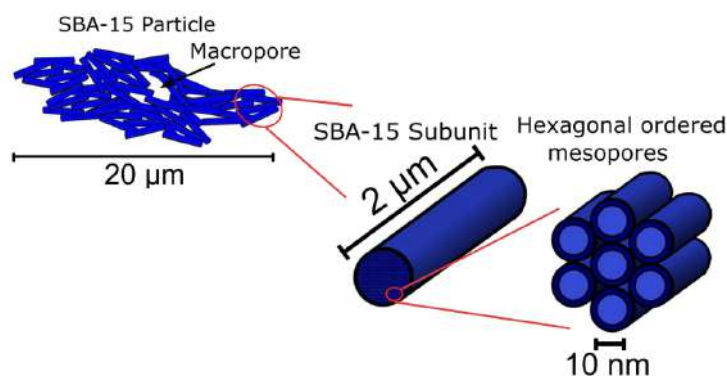


Figure 1.2: Scheme of SBA-15 structure extracted from Rasmussen et. al [12] showing the macropores and mesopores.

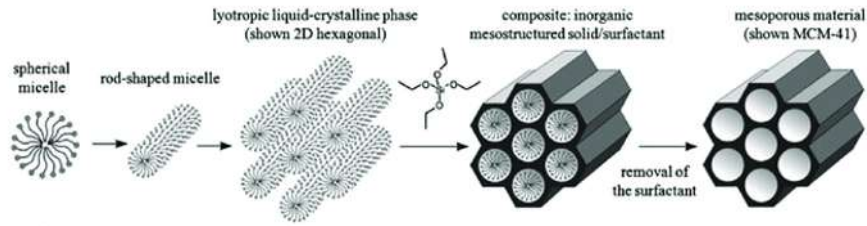


Figure 1.3: Scheme of SBA-15 synthesis extracted from [16].

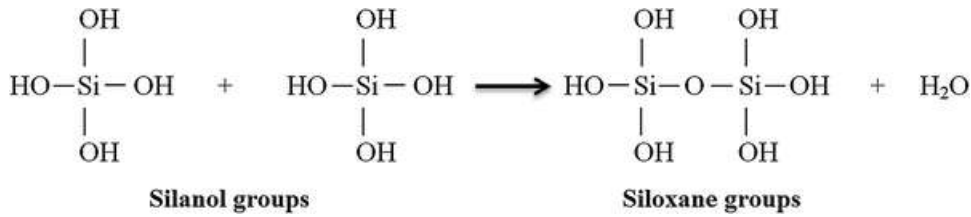


Figure 1.4: condensation of silanol groups to form a siloxane group extracted from [15].

The key features that make SBA-15 so advantageous as a nanocarrier for oral vaccines include: thick porous walls with mesopores, high surface area, ease of synthesis and functionalization, high thermal and mechanical stability and biocompatibility [19]. The protein adsorption into SBA-15 depends strongly on the antigen size and eventual clustering and it is highly affected by electrostatic and hydrophilic interactions [13, 20].

Environmental conditions, such as pH and ionic strength affect both the surface charge and charge density of the protein and SBA-15, which can in turn affect the protein's ability to bind to the surface of the mesopores and further incorporation [20, 21].

The pH is a logarithmic measure of the concentration of hydrogen ions in a solution [22]:

$$pH = -\log[H^+] \quad (1.1)$$

It ranges on a scale from 0 to 14, from acidic to basic solutions. An acidic solution has a higher concentration of hydrogen ions than of hydroxide ions ($[H^+] > [OH^-]$) and a pH lower than 7 and the opposite for a basic solution [22].

Ionic strength refers to the ion concentration in a solution and it is defined as [23]:

$$I = \frac{1}{2} \sum_i m_i \cdot z_i^2 \quad (1.2)$$

where m_i and z_i are the the molarity/molar concentration ($\frac{n}{V}$) and charge of each ionic species present in the solution.

Different studies reported a tendency that higher protein adsorption into SBA-15 is obtained when the solution's pH is close to the isoelectric point (pI) of the protein [20, 24, 21, 12]. At this pH, the proteins' net charge is zero, minimizing the repulsive electrostatic interactions between adsorbed proteins. This will allow them to pack closer to each other inside the pores and reach higher incorporation levels. Therefore, we expect a higher adsorption close to DT's pI (5.92¹). High ionic strength can screen electrostatic interactions, either they are repulsive or attractive, which tends to increase protein incorporation [20, 21]. Once high antigen concentrations are reached, there is a possibility that proteins might aggregate, which should be avoided. Ideally proteins should be uniformly distributed inside SBA-15's pores: this condition maximizes the contact between the antigen's surface and immune cells, inducing a stronger response [13]. Rasmussen et. al [3] investigated the use of SBA-15 for DT encapsulation and found that the mass ratio of 1:10 (DT:SBA-15) is the recommended ratio to avoid aggregation for pH 7.

Our focus is to optimize DT's intake into SBA-15, by changing the environmental conditions during adsorption, such as pH and concentration. Enhancing its uptake will produce higher antibody titers, which in turn will allow a stronger immune response [13]. We aim to find the optimal conditions by experimentally varying these parameters. We used 4 pH values and 7 different concentrations and a fixed ionic strength, in order to find its best combination. The choice for pH values used, was based on the pI of SBA-15 and DT and the point of zero charge (PZC) of SBA-15. PZC is the pH at which the surface charge density is null [25].

¹The isoelectric point of DT was calculated using the crystal structure of the toxin using ProtParam tool from ExPASy (Expert Protein Analysis System): <https://web.expasy.org/protparam/>. This value was not obtained from the anatoxin itself, but from the toxin, therefore there is possibly a deviation from the real DT's pI.

To start this pilot study, we used Lysozyme (Lys) to characterize the SBA-15, since SBA-15 morphology and origin affects the protein uptake [26]. Lys is a protein commonly produced by our body: it is present in mucosal secretions, such as tears, saliva and mucus and plays an important role in innate immunity [27]. Lys is a small globular protein with a molecular weight of approximately 14.4 kDa with dimensions of (3 x 3 x 4.5) nm and a pI value of 11 [21] (Fig. 1.5). It is a model protein for protein incorporation into SBA-15 and has been highly studied for this topic [19, 21, 20, 28]. On the other hand, as already mentioned, DT is a much bigger protein: it has a molecular weight of approximately 60 kDa and it is formed by elongated particles of 10 nm long and 3 – 4 nm wide [3] (Fig. 1.5).

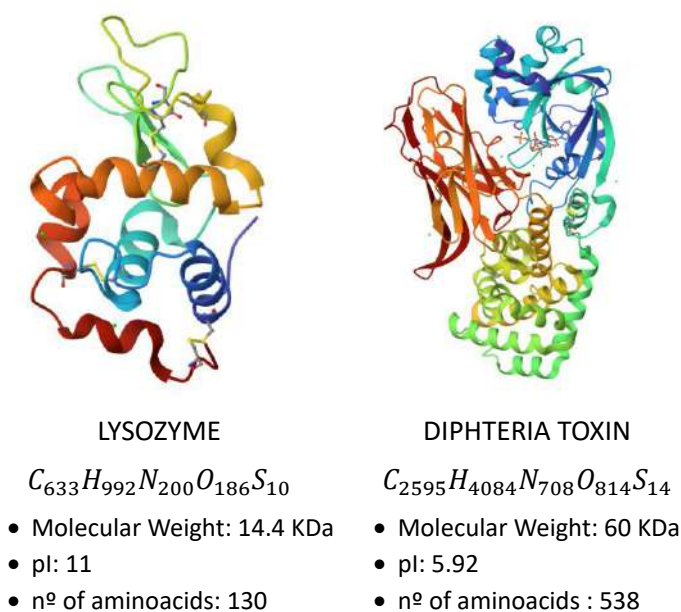


Figure 1.5: Structure of Lysozyme (left) and diphtheria toxin (right). Below it shows information on molecular weight, pI and n° of aminoacids for each protein. Structures images were taken from Protein Data Bank [29, 30].

Herein, for both Lys and DT, we defined adsorption as the mass of protein adsorbed per unit weight of SBA-15. Since this incorporation is performed in aqueous media, after incorporation, we need to separate the solid part (SBA-15 with incorporated protein) from the remaining liquid part (supernatant). In order to calculate the amount of protein adsorbed, we measured the protein concentration before and after incorporation, using UV-Vis spectroscopy. This technique measures light absorption, at the near UV and visible light

range. From the absorption level at 280 nm, it is possible to evaluate protein concentration [31, 32].

We proceeded to plot adsorption as a function of concentration (adsorption isotherm), after reaching equilibrium and at constant temperature. There are different models in literature that describe the shape of isotherms and how that shape can give us information about the adsorption dynamics going on for each specific adsorbate/adsorbent duo[33]. Based on literature results, we fitted our data to a Langmuir Model [19], from which we obtained parameters defining the thermodynamical process in question: affinity between adsorbate and adsorbant (K) and maximum adsorption (m_{max}). This model assumes that [33, 34]:

- There is no interaction between adsorbed molecules
- Adsorption sites are energetically homogeneous and independent
- Only one adsorbate molecule can bind to an adsorption site
- Adsorption process is dynamically reversible

The conditions for the Langmuir model lead to a very fast increase of adsorption for low concentrations, followed by a plateau (Fig. 1.6). This plateau is reached when all the adsorption sites are filled, forming a monolayer. Each point along the Langmuir curve is under dynamic equilibrium, therefore the rate of adsorption and desorption are equal.

We also analyzed the powder samples obtained after incorporation, using Thermal gravimetric analysis coupled to Fourier transform infrared spectroscopy and mass spectrometry (TGA-FTIR-MS). In the TGA technique, sample is decomposed by controlled heating. The result is a profile of mass loss as function of temperature or time. During sample decomposition, gases are released and coupling of MS and FTIR to TGA allows for a characterization of the evolved gases. From the FTIR, we obtain a light absorption spectrum, for the infra-red (IR) range and from the MS, a profile of the electric signal, associated to different mass to charge ratios (m/z) as a function of temperature or time. Combining all this information, we aimed to quantify the mass loss, recognize which reactions are happening for each temperature range and identify the material released during those reactions. This analysis allows us to understand if the material's decomposition is changing for the different pHs, that is, to check if there is any difference in the samples' environment [35].

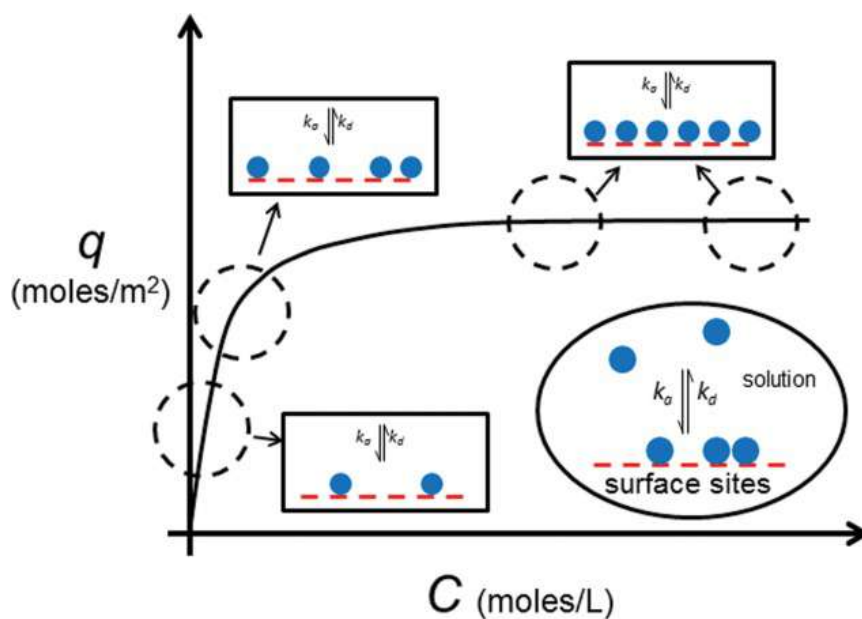


Figure 1.6: Plot of Langmuir model where $m_{protein}$ is shown as q . Blue circles and red lines represent adsorbent molecules and surface sites, respectively. It shows a very fast increase of q , until all adsorption sites are filled, reaching saturation. K_a and K_b (adsorption and desorption rate constants) represent a dynamic system under equilibrium. Figure extracted from [34].

This thesis is divided into introduction, materials and methods, results and conclusions and perspectives. In materials and methods, we describe Lys and DT's sample preparation, all the measurements performed on these samples, the techniques used and the methods used to analyse and fit the isotherms' data. Discussion and results show TGA-FTIR-MS measurement, the adsorption isotherm for the two proteins and respective parameters obtained by fitting the data to a Langmuir model. In conclusions and perspectives, we draw the general picture obtained from the experimental data and respective analysis and fitting procedures, as well as suggestions for further work on this topic, in order to improve our understanding of such complex systems.

Materials and Methods

2.1 Samples

The Lys used originated from chicken egg white (dialyzed, lyophilized, powder, 100000 U/mg) sourced by Sigma-Aldrich and used without further purification. The DT solution (dispersed in PBS buffer with a concentration of (7.00 ± 0.05) mg/mL) was donated by Instituto Butantan, São Paulo, Brazil. The SBA-15 used was provided by Institute of Physics, University of São Paulo, Brazil and prepared according to the procedure described on [36] for the sample named PO.

In order to maintain the desired pH and ionic strength constant throughout the incorporation, we prepared buffers: one for each pH, each with an ionic strength of 150 mM. The buffers were prepared by mixing the designated acid with sodium chloride in approximately 450 mL of water and then titrate the solution to the desired pH (Table 2.1)). The recipes were created using the website <https://www.liverpool.ac.uk/pfg/Tools/BufferCalc/Buffer.html> by choosing the desired parameters - see Appendix A. We used a Phosphate Buffered Saline solution (PBS buffer) to prepare Lys samples. The PBS buffer was prepared by dissolving one PBS tablet - Phosphate buffered saline P4417 Sigma-Aldrich - in 200 mL of water, which yields 0.01 M phosphate buffer, 0.0027 M potassium chloride and 0.137 M sodium chloride [37], which adds up to 150 mM ionic strength. This is a solution vastly used in biological research, in order to mimic the pH and ion concentration of the human body [37].

Table 2.1: Buffer nomenclature, acid used to prepare each specific buffer and mass of acid and salt used for preparation.

Buffer (pH)	Acid	Amount of acid (g)	Amount of NaCl (g)
Phosphate (2.9)	Phosphoric Acid (H ₃ PO ₄)	0.49	4.13
Acetate (5.6)	Acetic Acid (CH ₃ COOH)	0.30	4.13
Phosphate (7.4)	Monosodium Phosphate (NaH ₂ PO ₄)	0.60	3.64
CHES (9.1)	CHES free acid (C ₈ H ₁₇ NO ₃ S)	1.04	4.28

2.2 Sample Preparation

For SBA-15 characterization, we prepared 20 samples of Lys incorporated into SBA-15 at 10 different concentrations. For DT analysis, we prepared 64 samples: 16 samples for each pH series (4 pH series) and for each series, there were two samples with the same initial concentration and pH (first and second set). This approach aimed to check for result reproducibility. For each series of Lys and DT samples, we also prepared a control sample, which does not contain protein. This means that in this work a total of 84 samples were prepared.

We will name each sample, so that it is easier to follow the measurements performed. Lys samples will be named as P+ sample number (depending on the initial concentration used) + A or B (A referring to the first set of samples and B to the second) and DT samples are labeled as pH value + P sample number + A or B. Check Table 2.2 for the correspondence of sample number to its initial concentration. An example of this nomenclature is P2A and 7.4P2B : P2A means that we are referring to a Lys sample incorporated at a concentration of 2.5 mg/ml belonging to the first batch, while a sample named 7.4P2B refers to a DT sample prepared at pH 7.4 with a concentration of 1 mg/ml belonging to the second set of samples, batch B. The control samples will be referred as pH value + C + A or B, such as 9.1CA (control sample for pH series 9.1 for the 1st set of samples). For Lys control, it is named after the buffer used: PBS.

For the Lys samples, based on previous work [19], we expected to observe an adsorption curve similar to a Langmuir model. In order to obtain an accurate fitting, we tried to mainly place our data points in the curvature area (between the fast increase and the plateau of the model), by estimating which initial concentrations would allow it from the Langmuir fittings performed previously by our group [38]. For DT samples, the pH choice was based on SBA-15's PI (3.8) and PZC (5.2) and DT's pI (5.9): for pH 2.9, both materials are positively charged, pH 7.4 is close to SBA-15's PZC and DT's PI and within the pH range that both materials are oppositely charged and for pHs 7.4 and 9.1 both SBA-15 and DT are negatively charged, but pH 7.4 is closer to DT's pI than pH 9.1.

Table 2.2: Sample names for Lys and DT according to its pH and initial concentration. Lys samples will be named as P+ sample number (depending on the initial concentration used) + A or B (A referring to the first set of samples and B to the second) and DT samples are labeled as pH value +P sample number + A or B.

	pH	P + Sample # +	1st / 2nd set	Initial Concentration (mg/mL)
LYS	-	P1	A/B	2
	-	P2		2.5
	-	P3		3
	-	P4		3.5
	-	P5		4
	-	P6		5
	-	P7		6
	-	P8		8
	-	P9		11
	-	P10		12
DT	2.9/5.6/7.4/9.11	P1	A/B	0.5
		P2		1
		P3		1.5
		P4		2
		P5		3
		P6		4
		P7		5

For each sample we prepared 1 mL of protein solution (DT or Lys + designated buffer), the mass of protein added depends on each desired concentration, taking into account that Lys is in a powder form and DT in a solution. The steps further required to obtain this solution are explained below. Then, this solution was pipetted into approximately 10 mg of SBA-15 and everything was put into a thermomixer for 48h and afterwards centrifuged for 1 hour at 15000 rpm. Figure 2.2 shows the schematic of the procedure followed for sample preparation.

After centrifugation, the samples have a clear separation into solid and liquid phase (precipitate and supernatant, correspondingly). The solid phase is SBA-15 with incorporated protein and buffer salts inside its pores; the liquid phase is just the remaining protein dispersed in buffer solution. With a micropipette, we removed the supernatant from the solid phase, which was dried at 40 °C for 72 hours in an oven. Figure 2.3 shows the liquid and solid samples prepared according to this procedure. The protocol was adapted from Meissner et. al [24].

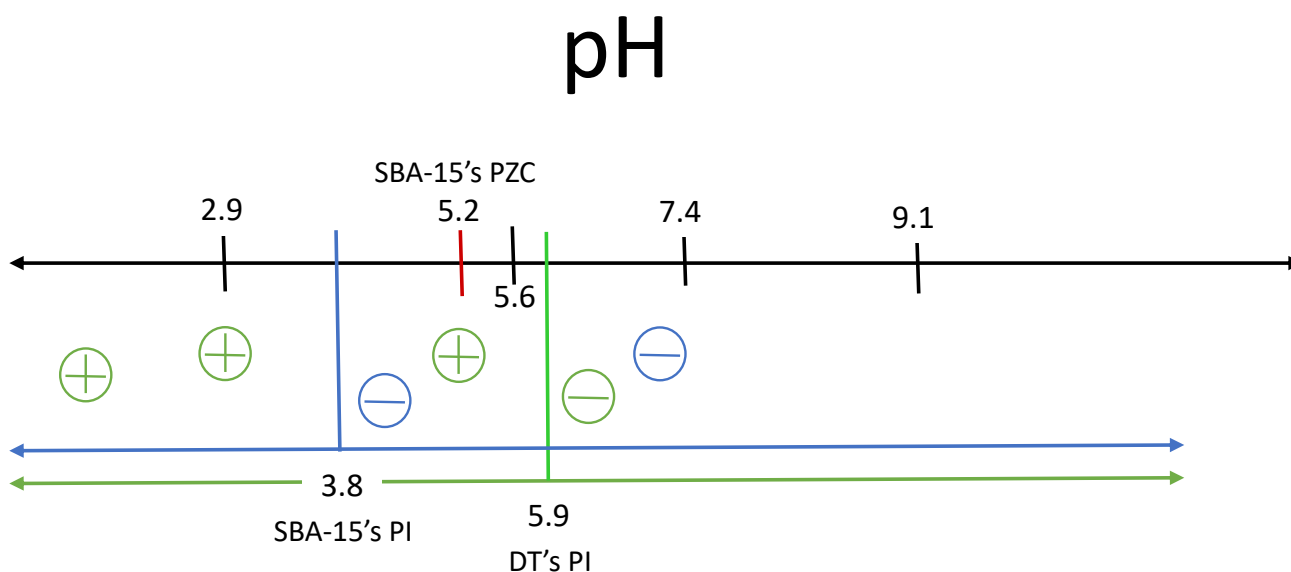


Figure 2.1: Black arrow bar shows the pH at which we performed incorporation (2.9, 5.6, 7.4, 9.1). Blue, green and red bar show the pI of SBA-15 and DT and PZC of SBA-15, respectively. Between SBA-15 and DT's pI, both materials are oppositely charged (SBA-15 is negative and DT is positive); Below and above this pH range, they are both positive (below) and negatively charged (above).

As mentioned before there are some steps required to go from the mother solution - the initial DT solution in PBS buffer - to a solution ready to use for sample preparation, that is, a buffer exchange. For each pH series, it is required 17 mg of DT (sum of all concentrations multiplied by the sample volume : $17 \cdot 1$). Since the mother solution has a concentration of 7 mg/mL, to prepare all the samples for each pH series, it is required 2.4 mL of mother solution, we purposely overestimated and considered 3 mL. We started by performing a buffer exchange: for each pH series, we placed 3 mL of mother solution into a concentrator tube with a molecular weight cutout of 30 kDa (this means that it will retain anything with a higher molecular weight than 30 kDa) and filled it up with the designated buffer, then we placed the tube in a centrifuge for 40 minutes at 6000 rpm. We repeated this process again: added more buffer into the concentrator tubes and centrifuged it, which leaves us with a very concentrated amount of DT. We proceeded to dilute in 3 mL of the corresponding buffer. We measured its concentration using the Nanodrop and performed the necessary dilutions in order to obtain the desired concentrations for each sample. These steps are shown in figure 2.4.

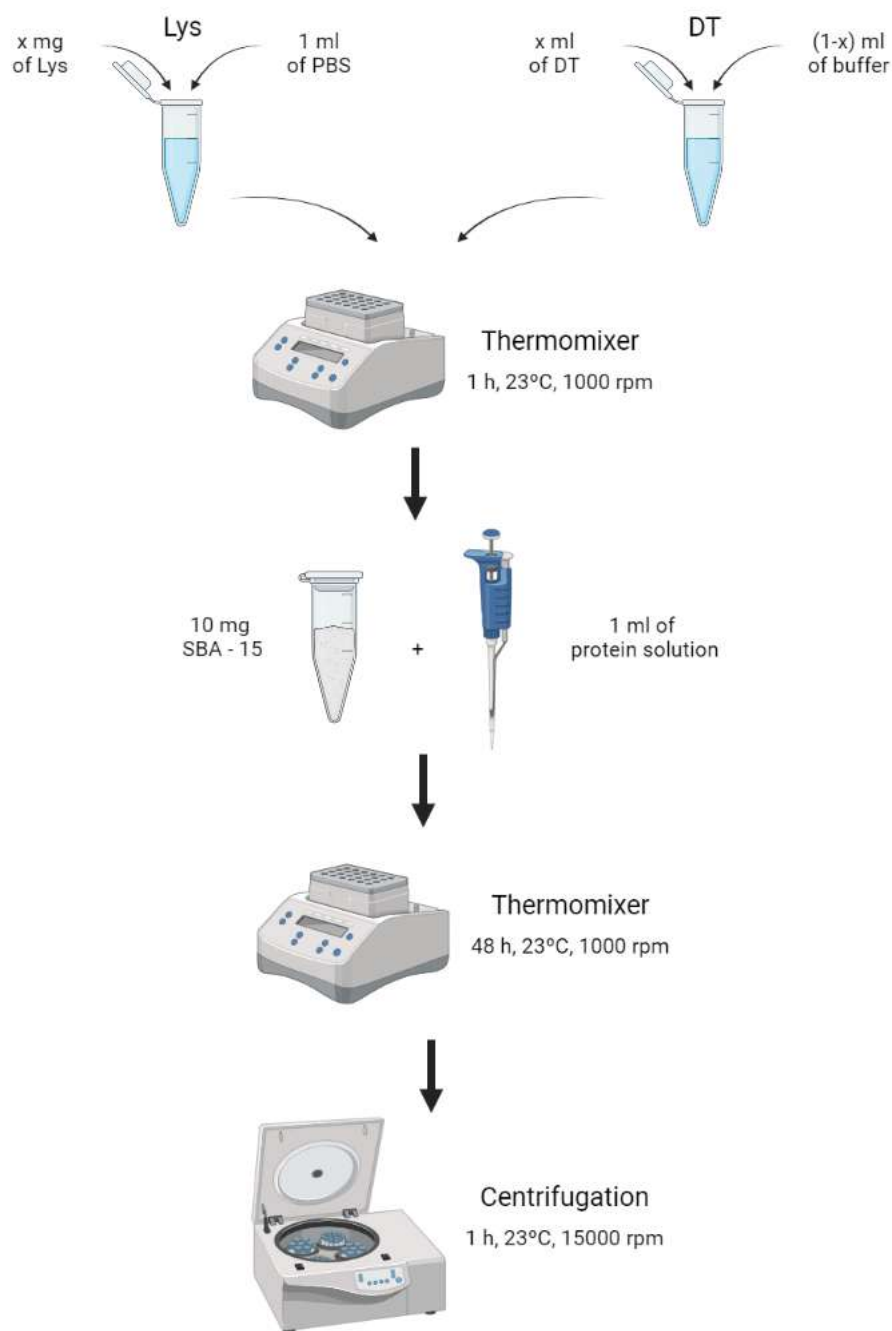


Figure 2.2: Scheme of sample preparation. Each sample was prepared by initially mixing a certain amount of protein with the corresponding buffer in a thermomixer and then mixing 1 mL of that solution to 10 mg of SBA-15, again, in a thermomixer, followed by 1 hour of centrifugation. Scheme created using BioRender.com.

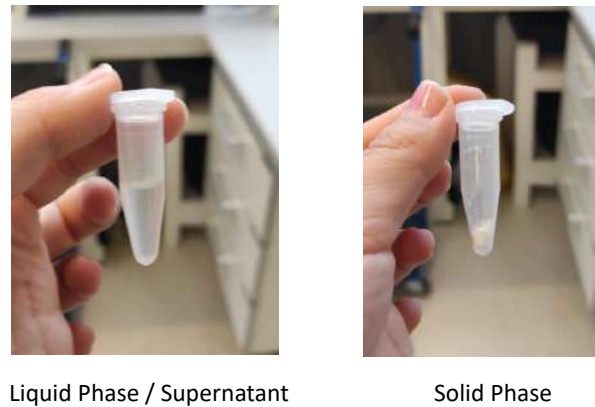


Figure 2.3: Image of liquid and solid phase after phase separation

For each buffer:

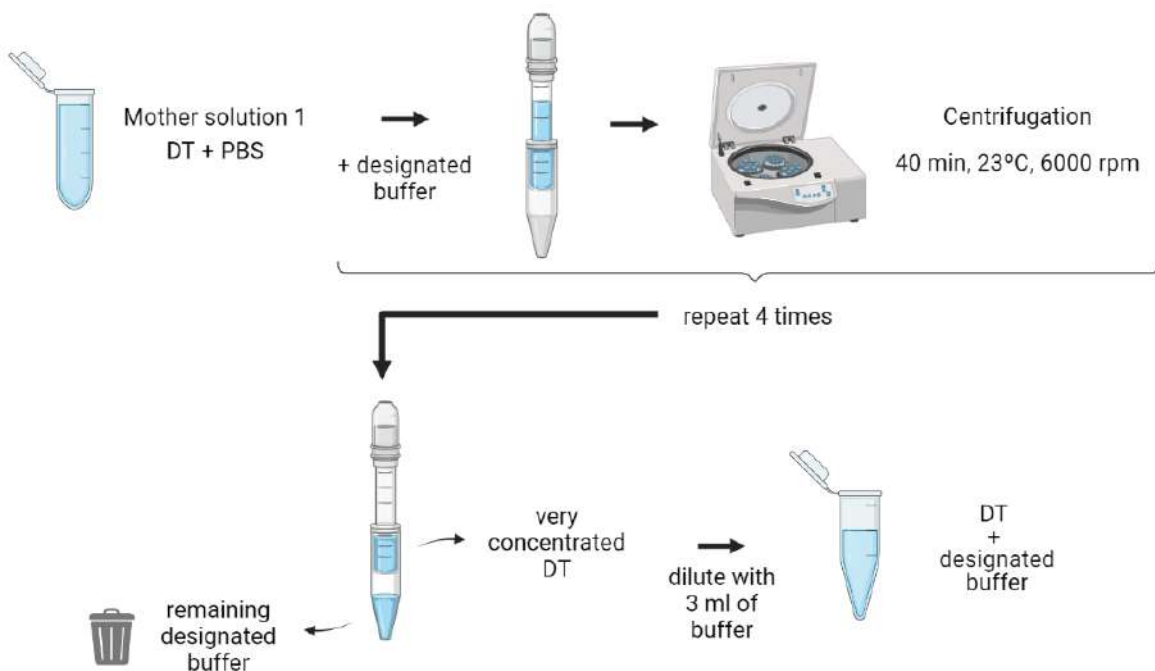


Figure 2.4: Scheme of buffer exchange protocol from mother solution (DT diluted in PBS) to a solution of DT diluted in the designated buffer. For each pH series, we centrifuged concentrator tubes containing a mix of mother solution and the assigned buffer, for 40 min. On the upper part of the tube, we have DT and below PBS buffer, that should be trashed. Afterwards we added more buffer and centrifuged and repeated this process one more time, until we have a very concentrated solution of DT on the upper part of the tube. To finalized, we diluted that in 3 mL of buffer and placed the solution in an eppendorf. Scheme created using BioRender.com.

Since DT's mother solution corresponds to a precious donation, we aimed to minimize the material loss. In this sense, we developed a protocol for the reuse of the non-incorporated protein, which allowed us to prepare the second set of samples. For each pH series, we placed the supernatant from the first set of samples into a container. Using a syringe and a 0.45 μm filter, we removed any remaining SBA-15. We concentrated the solution and washed it twice with PBS, using concentrator tubes. We diluted each concentrate in PBS and mixed the content from the 4 tubes into one vial, forming a mother solution 2. The obtained mother solution had a concentration of approximately 4.9 mg/mL. The repurposed DT was enough to prepare all samples except for 9.1P7. To make this sample, it was required one more round of DT reutilization. Under the assumption that pH would not affect the structure and integrity of the proteins, this procedure would allow us to mimic the conditions for the sample preparation of the first set of samples. This does not apply for Lys samples, only DT. A schematic of DT reutilization is shown in Fig. 2.5.

For each pH series:

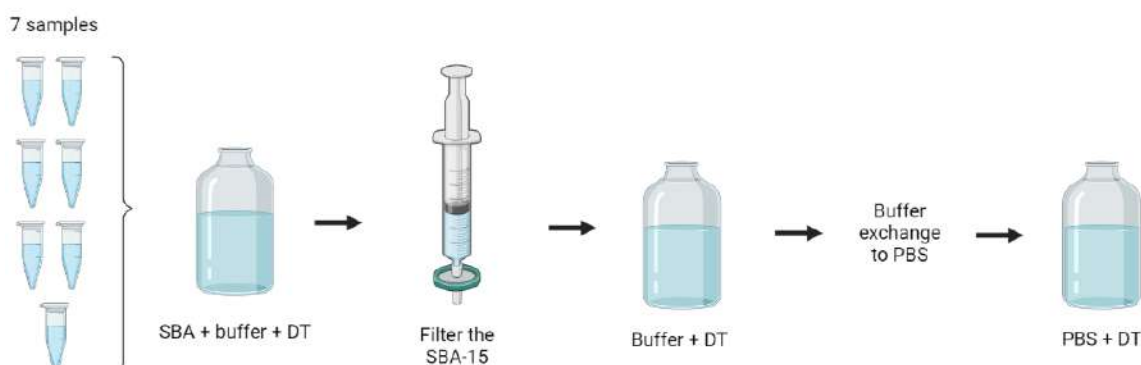


Figure 2.5: Scheme of DT reutilization protocol. For each pH series, we placed all the samples in a vial and filtered them using a syringe and a filter, in order to remove SBA-15 from the sample. Then, we performed buffer exchange to PBS, this way, we obtain a solution of DT diluted in PBS. Scheme created using BioRender.com.

2.3 Protein Adsorption Measurements

Protein concentration is evaluated from UV-Vis measurements, while the specific adsorption/protein intake capacity (A) is calculated as [24]:

$$A = \frac{m_{prot}}{m_{SBA-15}} = V \cdot \frac{C_i - C_f}{m_{SBA15}} \quad (2.1)$$

where V is the volume of protein dispersion (1 mL), m_{prot} and m_{SBA-15} are the protein and SBA-15's mass, respectively. The initial concentration (c_i) refers to the protein concentration before SBA-15 addition of SBA-15, while final concentration (c_f) refers to the protein concentration measured from the supernatant, after incorporation.

2.3.1 Basics of UV-Vis spectroscopy

UV-vis spectroscopy is a simple, non-destructive method that measures light absorption by the solution as a function of wavelength. It works at the near-ultraviolet (near UV) range (200 to 400 nm) and the visible range (UV-Vis) (400 to 750 nm). Light absorption spectrum fully depends on sample composition. Thus, absorption spectrum can provide information on sample composition and concentration [31].

When a molecule absorbs a photon, it gets excited from its ground state to an electronic excited state. This process requires that the photon energy corresponds to the energy difference between these states - this energy is typically within the near UV to UV-Vis range[31].

The key components of a UV-Vis spectrophotometer are a light source, a monochromator, a sample and reference cells and detectors [39]. The light is emitted from the source and passes through the monochromator, which is composed by a slit (in order to orient the light rays), a dispersion device (to separate the light into its wavelengths) and another slit (that works as a wavelength selector). The beam moves on to a beamsplitter, forming two equivalent and parallel beams: one goes through a reference cell and the other through a sample cell and both get detected, by different detectors (Fig. 2.6). The first detector measures the incident light and the latter the transmitted light.

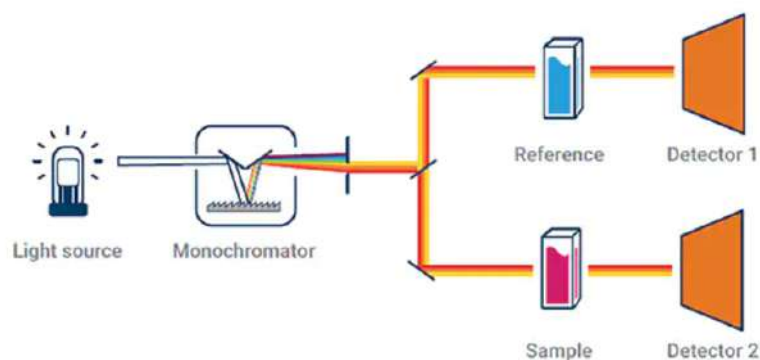


Figure 2.6: Scheme of UV-Vis spectroscopy set up extracted from [40].

Using the Beer-Lambert law, to the absorption at 280 nm, we can obtain the sample's protein concentration [41]:

$$A = \log_{10} \frac{I_0}{I} = \epsilon \cdot l \cdot C = \epsilon \cdot l \cdot \frac{c}{M} \quad (2.2)$$

where A is the absorbance and I_0 and I are the incident and transmitted intensity; ϵ is the extinction coefficient or molar absorption coefficient, l is the optical path and C is the molar concentration, which corresponds to the protein mass concentration (c) divided by its molar mass (M).

Protein concentration is typically measured at 280 nm, because at this wavelength, aminoacids, in particular, Tyrosine, Tryptophan and Cysteine, strongly absorb UV light[40]. In fact, the extinction coefficient at 280 nm can be calculated as the sum of the molar absorption coefficients of the three aminoacids at this wavelength [32]:

$$\epsilon = n_W \cdot 5500 + n_Y \cdot 1490 + n_C \cdot 125 \quad (2.3)$$

where n_W, n_Y and n_C are the number of Tryptophan, Tyrosine and Cysteine aminoacids for each protein and the stated values are the respective molar absorptivities at 280 nm.

The resulting spectrum is presented as a graph of absorbance as a function of wavelength.

We used the Thermo Scientific NanoDrop 1000 Spectrophotometer and measured protein absorption at 280 nm. For the initial concentration, we used the corresponding buffer as background and for the final concentration, we used the control sample of the same pH set. Table 2.3 shows the molecular weight and extinction coefficient for Lys and DT.

Table 2.3: Information on molecular weight and extinction coefficient for each protein used in this work.

Protein	Molecular Weight (KDa)	$\epsilon((M^{-1}cm^{-1}) \cdot 1000)$
DT	60.2	54.4
Lys	14.4	24.6

For each measurement, we placed a drop of solution (around 3- 4 μ l) on the designed place on the lower support and rinsed twice between each measurement.

2.3.2 Adsorption isotherm Fit

After measuring concentration, we calculated specific adsorption and plotted an adsorption isotherm for proteins incorporation into SBA-15 at each pH. Based on results obtained by Meissner et. al [19], that used the Langmuir model to fit the adsorption isotherm of Lys incorporated into SBA-15, we used the same model to fit our data.

Based on the underlying requirements for a Langmuir model, defined in introduction (equivalent and homogeneous adsorption that can only bind to one adsorbant molecule, no interaction between adsorbed molecules and adsorption is a dynamic reversible equilibrium process), we can define the adsorption reaction as [34, 42]:



where A, V , and A^* ($A \cdot V$) represent the adsorbate molecules, available adsorption sites and the adsorbed molecules or occupied adsorption sites, respectively, and k_a and k_d represent the kinetic rate constants of adsorption and desorption, respectively. Let us define θ as the ratio between occupied sites (N) and the total number of adsorption sites (M), which is the same as the ratio between mass of adsorbed molecules and mass of maximum proteins possibly adsorbed to the adsorbate (when saturation and monolayer is reached) and C the adsorbate concentration. The overall rate of adsorption is defined as the rate of adsorption minus the rate of desorption. The first is the rate at which a molecule binds to an empty site and the latter the rate that a molecule is released from a site.

$$\frac{dA^*}{dt} = K_a \cdot C(1 - \theta)M - K_d \cdot \theta M \quad (2.5)$$

For equilibrium conditions $\frac{dq}{dt} = 0$ and $K = \frac{K_a}{K_d}$. Rearranging the equation, we have:

$$\theta = \frac{C \cdot K}{1 + C \cdot K} \quad (2.6)$$

In the context of protein adsorption into SBA-15, the Langmuir equation can be written as [33]:

$$m_{prot} = m_{max} \cdot \frac{K \cdot c_{eq}}{1 + K \cdot c_{eq}} \quad (2.7)$$

where $\theta = \frac{m_{prot}}{m_{max}}$. m_{prot} and m_{max} are the mass of adsorbed protein and the maximum uptake possible and c_{eq} is the equilibrium concentration and K is the Langmuir equilibrium constant, which defines the affinity between protein and SBA-15. m_{max} is highly dependent on pH and salt concentrations, while K depends mainly on the interaction between adsorbant and adsorbate. These parameters characterize the thermodynamics of the adsorption process [34].

In order to understand how well the Langmuir model fits our data, we used the least squares method from Curve_Fit (a package in Python) [43], which

returns an estimate and error for all parameters of the fit. To measure the goodness of fit we used a reduced χ^2 test. The reduced χ^2 value is calculated as [44]:

$$\chi_r^2 = \frac{1}{dof} \sum \frac{(O_i - E_i)^2}{E_i^2} \quad (2.8)$$

where O_i is the observed value and E_i the expected value, which is the value obtained using the fit equation. dof corresponds to the number of degrees of freedom (number of data points minus number of fit's parameters). The closer this value is to 1, the better is the fit.

2.4 Thermal Analysis of samples

We performed Thermogravimetric analysis coupled to Fourier transform infrared and mass spectrometry (TGA-FTIR-MS) of the solid dried samples, in order to analyze the samples in its powder form, this way we get to understand if and how the environment is changing for different incorporation.

2.4.1 Basics of TGA-FTIR-MS

- TGA

Thermogravimetric Analysis (TGA) is an experimental technique in which we track a substance's mass as a function of temperature and time, on a controlled atmosphere. It is used in a variety of fields, such as environmental, food science, pharmaceuticals and others, in order to characterize materials and study its stability and composition [45, 46].

The temperature can be set to different programs, depending on what is most suitable for the experiment, that is, the type of information we want to gain. Temperature can either increase at a constant heating rate or with a non linear temperature program (dynamic measurement), it can be maintained constant throughout the experiment (isothermal measurement) or it can increase in sequential steps, so that the sample mass

can stabilize between steps. It typically varies from ambient temperature ($\sim 25\text{ }^{\circ}\text{C}$) to $1000\text{ }^{\circ}\text{C}$. The atmosphere can also be a varying parameter for experiments: the atmosphere is controlled by introducing a purge gas: this gas can be reactive, oxidising (such as air or oxygen) or inert (such as nitrogen, argon, or helium) or even change throughout the measurement [46, 35].

The results are displayed as a TGA curve on the computer. This curve shows the percentage mass loss as a function of time or temperature. By plotting the first derivative of this curve (dTGA or DTG curve), which represents the rate of mass change, we have a better visualization of the time/temperature at which there is a higher change in mass (a step in the TGA curve will result in a peak in the dTGA curve). This mass change can either be a gain (this could be caused by oxidation or adsorption/absorption, for example) or a loss. There are a lot of possibilities for the cause of mass loss, depending on which material we are analysing and the atmosphere set, such as, evaporation, thermal decomposition, desorption and dehydration, for example [35]. We can also obtain the mass loss by integrating the dTGA curve (area below the curve). For calculation of protein % present in samples, we averaged the value obtained by the TGA directly (subtracting final to initial mass loss) and by the area below the dTGA curve.

In order to start the measurements, a crucible containing the sample is placed on a platform. This platform is connected to a thermobalance: a precision electronic microbalance, located inside a furnace with a temperature programmer and controller. During the measurement, the balance weighs the sample in a closed furnace. A purge gas is introduced into the chamber, in order to control the atmosphere and a protective gas to protect the balance from potential corrosion [47, 45].

For TGA measurements, it is very important to take into account buoyancy effects. If we do not, our results will show a false mass increase, because density of gases change with temperature: $\rho = \rho_0 \cdot \frac{T_0}{T}$. Therefore, for buoyancy correction, a blank measurement should be performed: a measurement using an empty crucible and the same temperature and gas program. This curve is used as background and subtracted from the following measured curves (with sample) [35].

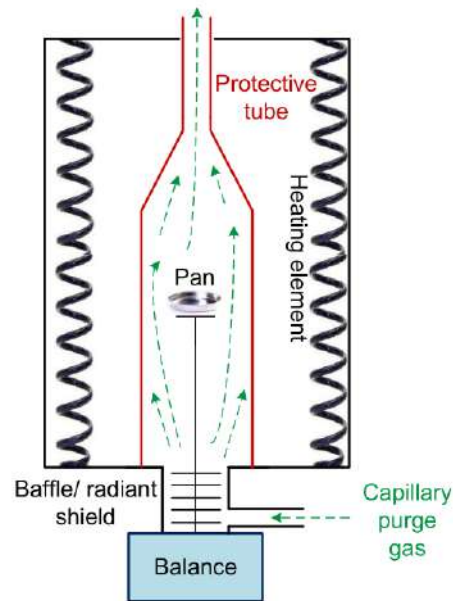


Figure 2.7: Scheme of TGA's thermobalance extracted from [47].

When analyzing the obtained results, it is important to consider certain factors that influence the measurements, such as [35]:

- Method parameters:
If the sample undergoes chemical reactions, the temperature range for the reaction depends on the heating rate. If the heating rate is slow, it allows for the sample to reach equilibrium, otherwise it creates a thermal lag.
The type of gas and gas flow set for the measurement will also affect the results.
- Sample size, homogeneity and morphology:
Sample mass also affects the results of the measurement - if the mass is too high it can lead to a less accurate representation of the thermal behaviour of the material; if it is too small, it will lead to a higher signal to noise ratio.
The sample should be prepared to ensure homogeneity, avoid contamination, and avoid changes to the sample during analysis.
- Evolved Gas Analysis (EGA)

We are able to identify and analyse the nature of the gases released from the TGA, by combining this instrument with EGA. We use a mass spectrometer (MS) and Fourier transform infrared spectrometer (FTIR) coupled to the TGA [45]. Both FTIR and MS are substance specific, which means that, each substance has a specific MS and FTIR spectrum, that can be recognized as their own [35]. It is very useful, to have information from both the MS and the FTIR, because we can connect the two measurements and easily get a more clear insight of sample's composition. We will mainly keep track of water and carbon dioxide profiles, both from the MS and FTIR (Table 2.4 and Fig. 2.10). CO_2 is a marker for protein degradation in this context, therefore the CO_2 profile, allows us to understand the protein degradation profile. Water is important in many aspects for further thermal analysis:

- Water in SBA-15

Water dynamics, either surface and confined water in SBA-15, is important under this context: since incorporation happens in an aqueous medium, diffusion rules how proteins and salts are incorporated into SBA-15's pores [48, 49].

- Water in Proteins

Water tends to form hydrogen bonds with aminoacids, which is important for packing and stabilization of its structure, by exposing hydrophilic patches and hiding hydrophobic patches [50, 51]. Therefore, proteins have water attached (bound water) to its structure, but also loosely bound water attached to its surface.

- MS

MS is a technique able to detect and measure the mass-to-charge ratio (m/z) and its relative abundance, of one or more molecules present in a sample [52]. This technique can be used to identify different compounds by its molecular weight and to quantify the amount of each compound in a sample [35].

When coupled to the TGA, the gas evolved from the TGA is transported, through a gas outlet, from the chamber to the MS. Once entering the MS, the gas molecules are bombarded with electrons, at the ion source,

causing molecules to fragment [35]. Molecules can fragment in different ways, based on their structure and therefore form fragments with different molecular weights. The fragments formed are accelerated into a magnetic field and a certain velocity is selected for analysis: when encountering a magnetic field, any charged material deflects its trajectory and the amount of deflection depends on its mass and charge. Because the fragments move with a direction perpendicular to the magnetic field, their trajectory will follow a circular path until they hit the detector (Fig. 2.8). From the radius of curvature, we can gain information on its mass to charge ratio [35, 53]. That means we have a centripetal force caused by the magnetic field, therefore we can say that centripetal force (F_C) is equal to the magnetic force (F_M), this way we can relate the radius of curvature to m/z [54]:

$$F_M = F_c \iff q \cdot v \cdot B = \frac{m \cdot v^2}{r} \iff r = \frac{m \cdot v}{q \cdot B} \quad (2.9)$$

where q is the charge of the fragment, v is the velocity and B is the magnetic field. In this equation, $\frac{m}{q}$ represents the mass to charge ratio (m/z). We can obtain the radius of curvature by detecting where the fragment hits the detector [35, 53].

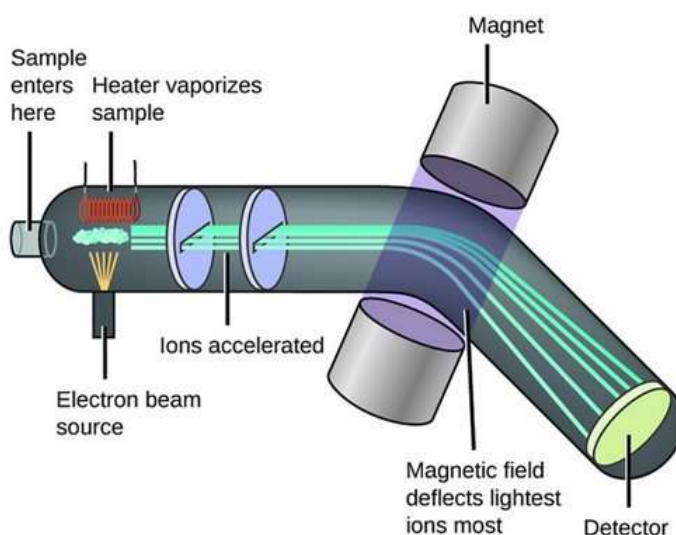


Figure 2.8: Scheme of Mass spectrometry extracted from [53].

These measurements are displayed in a computer as a mass spectrum (relative abundance as a function of m/z). Since some fragments are more stable than others, then the more stable fragments will be more

likely to form and they will show higher peaks. From this spectrum we can gain some knowledge on the sample's constituents. For the TGA coupled to the MS, the data is displayed as signal intensity (ion current) as a function of time or temperature, for each m/z . We can select the m/z of interest and visualize its curve on top of the TGA and DTG curves. This way we can correlate the two measurements and have a better understanding of which compounds are being released at each step and what reaction is leading to their release [46]. Table 2.4 shows the relative of intensities for H_2O and CO_2 .

Table 2.4: Table of MS relative intensities of H_2O and CO_2 . Adapted from [55].

m/z	Relative intensities	
	H_2O	CO_2
12		6.7
16	1	9.5
17	21	
18	100	
22		1
28		8.2
29		1
44		100

- FT-IR

Infrared (IR) spectroscopy is one of the most commonly used spectroscopic techniques. IR spectroscopy measures the light absorbed by molecules at the IR range. In this region the absorption is due to rotation and vibration of molecules [56]. Molecular vibrations are classified into stretching (change in distance between atoms that share a bond) or bending (change in angle between atoms that share a bond). Bending includes scissoring, rocking, wagging, and twisting [57]. Absorption occurs when the frequency of vibration matches the frequency of incident radiation and it results in amplitude change of the vibration [56].

The main components of an FTIR are a source, interferometer and detector. The difference between FT-IR and IR is in the use of a Michelson interferometer[56] (Fig. 2.9). IR radiation is emitted from the source, it goes through a collimator (forms parallel rays), in order to reach the interferometer. A Michelson interferometer is composed by a beamsplitter and two perpendicular mirrors (one movable and one fixed). Inside the

interferometer, light reaches the beamsplitter: the transmitted light and the reflected light strike the stationary mirror and the movable mirror, respectively. The light is reflected by the mirrors and recombined at the beamsplitter. Since one of the mirrors is moving, there will be an optical path difference between the two beams and the intensity of the recombinant beam will fluctuate between maximum amplitude (situation of constructive interference) and 0, destructive interference. The recombinant beam reaches the sample and it is detected by the detector. This data is displayed as amplitude (measured in V) as a function of OPD (measured in terms of time, which will look like a cosine function[56].

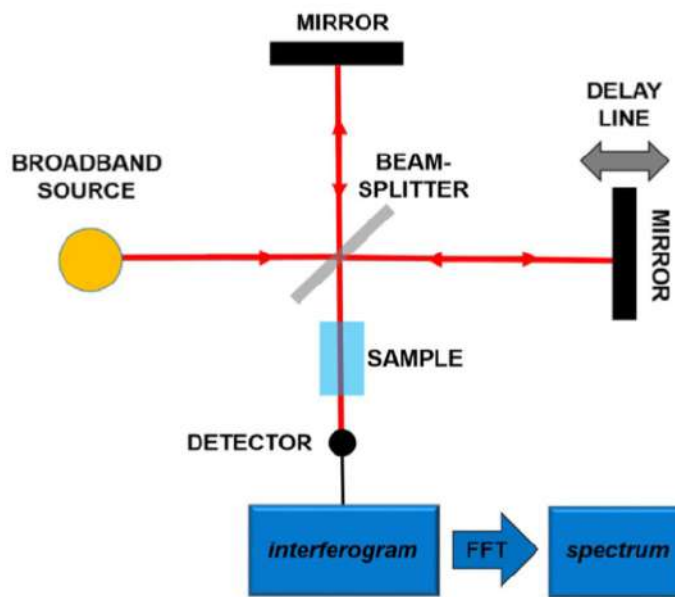


Figure 2.9: Scheme of FT-IR extracted from [58].

The time domain is Fourier transformed to get a frequency domain. Fourier transform is a technique that transforms a function of time $x(t)$ to a function of frequency $X(W)$:

$$X(w) = \int_{-\infty}^{\infty} x(t) \cdot e^{-j\omega t} dt \quad (2.10)$$

The frequency is directly proportional to the wavenumber:

$$c = \lambda \cdot \nu \quad (2.11)$$

where c is the speed of light, λ is the wavenumber and ν is the frequency.

Therefore, we can construct a plot of intensity (intensity is directly proportional to amplitude) as a function of wavenumber. When comparing the difference between the incident and emitted radiation, for each wavenumber we get a spectrum of absorbance (%) as a function of wavenumber [56].

The coupling of TGA to FT-IR, just like the MS, allows us to identify functional groups present in the evolved gases. Since each molecule has a characteristic spectrum (fingerprint), we can compare the obtained spectra to a data bank containing a variety of substances, which allows us to identify the different constituents of the evolved gas, in question. Common groups with characteristic absorbances include aldehydes, ketones, esters, alkenes, alkynes, alcohols, amines, amides, carboxylic acids, nitro groups, and nitriles.[56, 59, 57]. Fig. 2.10 shows the FTIR spectrum of CO_2 (top) and H_2O (bottom).

We used a Perseus TG 209 F1 Libra (Netzsch, Germany) TGA coupled to an ALPHA FTIR spectrometer (Bruker Optics Inc., Germany) and a QMS 403 Aëolos Quadro (Netzsch, Germany) MS. All measurements were performed in aluminium oxide crucibles without lids, to which we added between 2 to 4 mg of the material we wanted to analyse, approximately. We set a heating rate of 10 K/min and used a 20 ml/min for the purge and protective nitrogen gas flow. For the Lys samples, we measured until 450 °C and for DT and control samples both 450 and 1050 °C. For pure SBA-15 samples, we performed measurements from room temperature to 450, 900 and 1050 °C. For some of the Lys sample measurements, we also set an isotherm: we increased the temperature from 28 to 40 °C with a 5 K/min rate and then set an isotherm for 30 minutes at 40 °C, followed by a 10 K/min increase in temperature until 450 °C, as an attempt to reduce surface water.

Some of our FTIR measurements, show an oversubtraction of the background measurements for CO_2 and/or H_2O - that should not be considered as signal, only peaks above the baseline should be considered. These are abundant molecules and the instrument is able to detect any change in the laboratory conditions, due to its sensitivity. The IR spectral range is of 500 to 4500 cm^{-1}

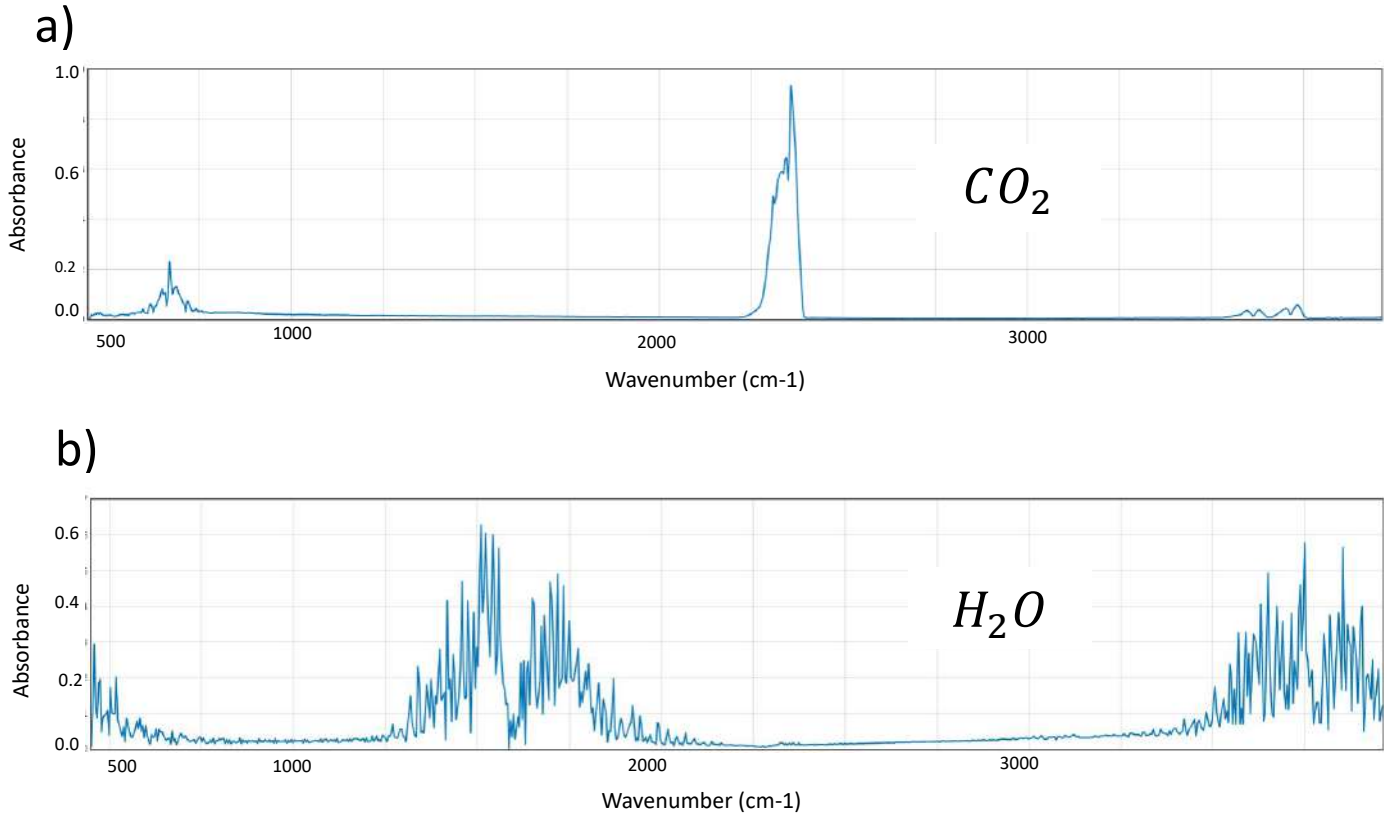


Figure 2.10: FTIR spectrum of CO_2 (top) and H_2O (bottom). Adapted from [60] and [61], respectively.

and spectra is collected every 3 minutes. The MS spectra was collected every 0.005 seconds for a m/z range of 1 to 50.

On the TGA Perseus software is possible to smooth the different curves we obtain. The data shown in this report, for the TGA and DTG curves, has been smoothed, because the data was too noisy. This noise arrives mainly from the sample's porosity and non homogeneity. The smoothing was done taking into account that the source of error is from the sample's nature and that the smoothing cannot change the curve trend and features.

Results and Discussion

3.1 SBA-15 characterization

Fig. 3.1 shows the TGA and dTGA curves (on top) and MS at $m/z = 18$ and 44 (below) of pure SBA-15 from room temperature to 1050 °C. The TGA curve shows 3 subtle mass loss steps: from room temperature to 100 °C, there is a 0.5 % mass loss, then the curve plateaus and from 225 °C to 750 °C, there is a 3 % mass loss, finally, from 750 to 1050 °C, the curve becomes less steep and the sample loses 0.5 % of its mass. Summing it all up, there is an overall mass loss of 4 %. Taking a closer look into the dTGA and MS: we observe a first and second dips at 50 and 350 °C in the dTGA accompanied by peaks at the same temperatures in the $m/z = 18$ signal, which suggests water loss. These are two different water species, differentiated by how attached the water is to the SBA-15 structure. Since the first peak appears at low temperatures and the second at higher temperatures, the first corresponds to superficial water and the latter to bound water. The $m/z = 44$ signal is low until 300 °C, it shows a small peak at 500 °C and a fast increase above 750 °C. A high $m/z = 44$ denotes the presence of carbonaceous materials and its degradation. Recalling the SBA-15 synthesis, the only carbonaceous material is the organic polymer used to form micelles. Therefore, this signal shows the presence of leftover polymer calcination in the SBA-15 sample in question [62]. The fast increase in the $m/z = 18$ signal is a byproduct from polymer degradation: the loss of adsorbed water attached to the polymer chains. The FTIR spectrum (Fig. 3.2) exhibits a constant water signal that is gradually increasing from 100 to 1000 °C, which is in agreement with a high $m/z = 18$ signal throughout the whole temperature range. The carbon dioxide signal appears at 900 °C (for lower temperatures there is oversubtraction), which, again, agrees with the $m/z = 44$ high signal at temperatures above, approximately, 800 °C.

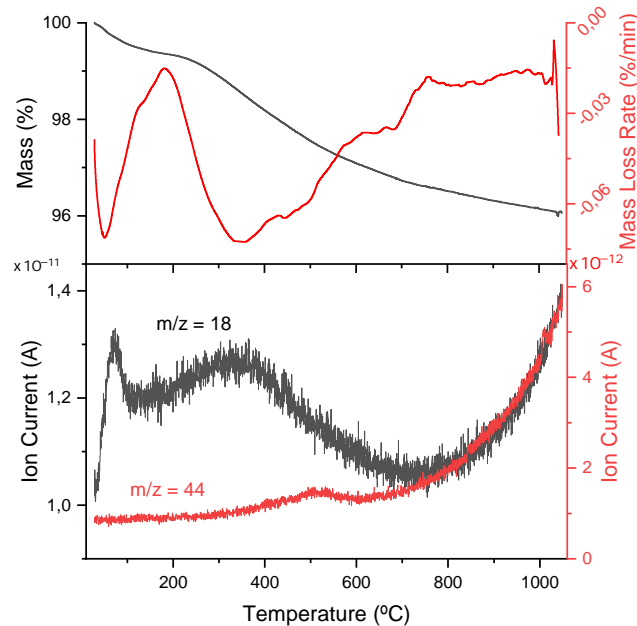


Figure 3.1: Top: TGA (black) and dTGA (red) curves of SBA-15 from room temperature to 1050 °C. Bottom: MS at $m/z = 18$ (black) and 44 (red). Note that the ion current is much smaller for the CO_2 response (CO_2 y-axis is on the scale of 10^{-12} , while for water is in the scale of 10^{-11}) indicating smaller amount of CO_2 than water in the system.

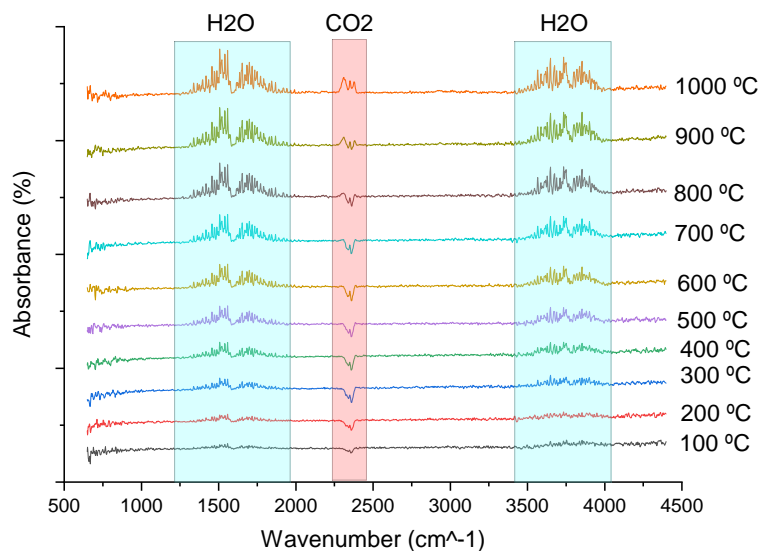


Figure 3.2: FTIR spectra of SBA-15 from 100 to 1000 °C in steps of 100 °C. Blue and red rectangles highlight the presence of H_2O and CO_2 , respectively: CO_2 is present above 900 °C and H_2O throughout the whole temperature range, with different intensities.

In order to get an insight on sample homogeneity, we performed 3 TGA-FTIR-MS measurements on SBA-15: SBA-15 1, 2 and 3 (Fig. 3.3). The mass of each sample is shown in a table in Appendix G. Both TGA, dTGA and MS at $m/z = 18$ show differences between samples, therefore the SBA-15 might not be completely homogeneous, but overall all curves present the same trends described above (Fig. 3.1). These differences can be, in part, explained by taking into account that the measurements were not performed on the same day (slightly different atmospheres), the differences in the MS are in the scale of 10^{-11} and 10^{-12} (see Appendix B for the non normalized MS plots), the samples have different masses, and it is a porous material.

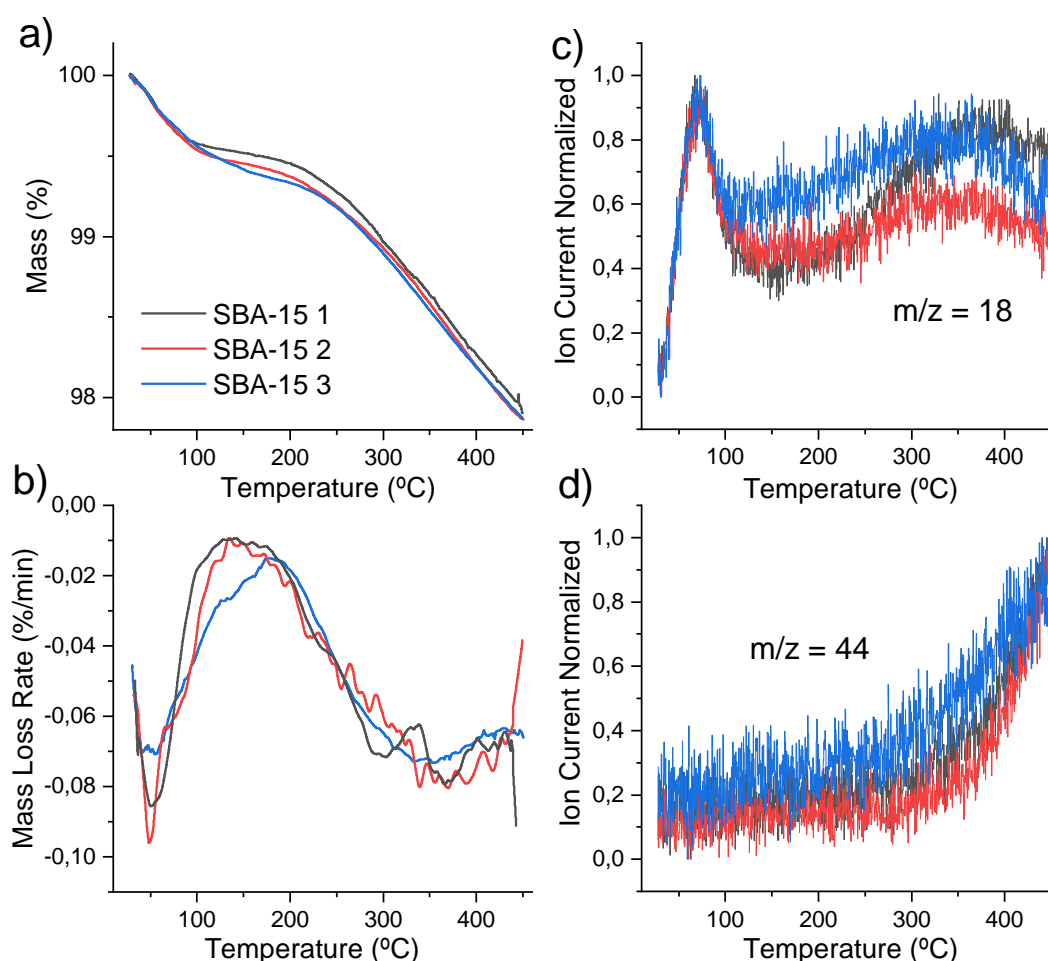


Figure 3.3: Comparison between SBA-15 1 (black), 2 (red) and 3 (blue) of a)TGA curves, b)dTGA curves, c)MS at $m/z = 18$ and d) $m/z = 44$.

3.2 Lysozyme Results

3.2.1 Lys adsorption into SBA-15

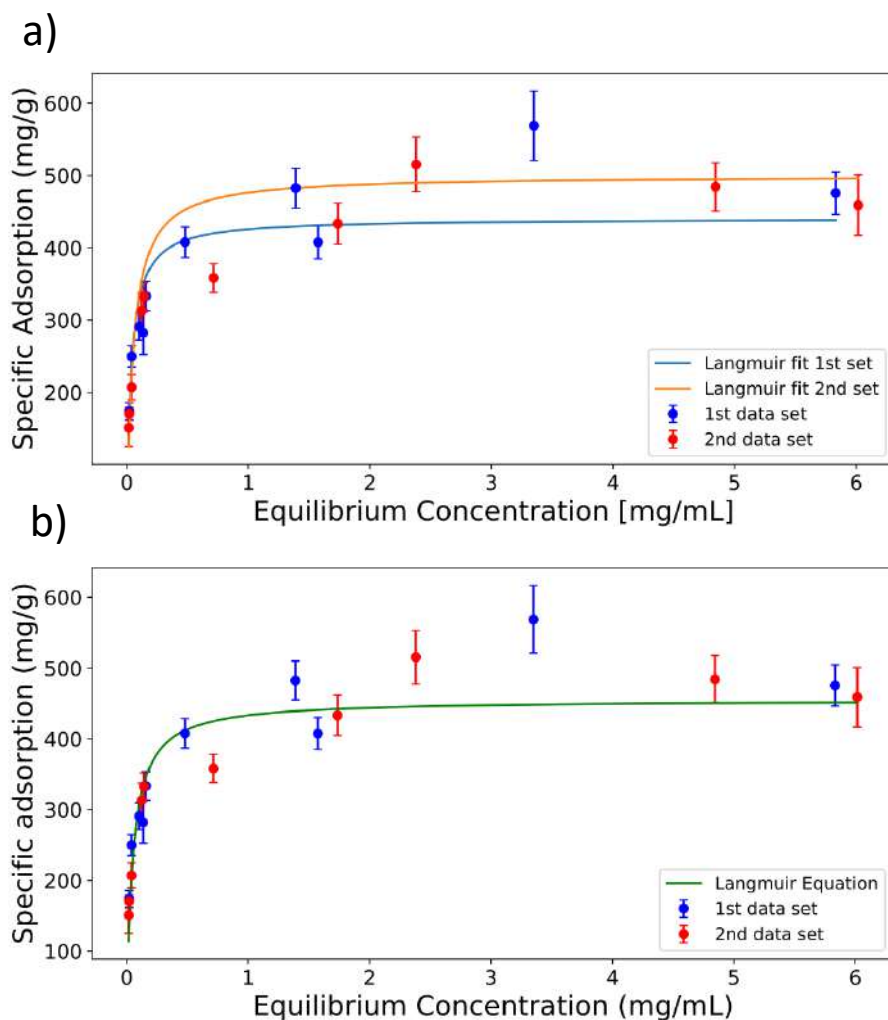


Figure 3.4: Adsorption isotherm of Lys into SBA-15 and Langmuir fit for first and second data sets (a). Adsorption isotherm of Lys into SBA-15 of first and second data points and Langmuir fit of the merged data sets (b). Circles correspond to experimental points, vertical lines are the errorbars and full line are the fitted data.

We started by attempting to reproduce previous literature results with adsorption of Lys into SBA-15, so that we would have a baseline comparison for DT adsorption.

Table 3.1: Table of fitting parameters for 1st, 2nd data set and all data points: K , m_{max} and χ_r^2 .

	1st data set	2nd data set	merged data sets
K	28 ± 3	30 ± 3	23 ± 3
m_{max}	441 ± 12	426 ± 13	443 ± 10
χ_r^2	3.5	2.7	2.6

Our results for Lys incorporation into SBA-15 with PBS buffer ($\text{pH} = 7.4$) for different concentration are plotted in Fig. 3.4: it shows the specific adsorption (mass of Lys per 1 g of SBA-15) as a function of equilibrium concentration (final concentration obtained from the supernatant) for first and second data sets. For both data sets, we can observe a very fast increase initially and around 1 mg/ml, it reaches a plateau. This behaviour resembles a Langmuir isotherm with a high affinity between Lys and SBA-15's surface. We fitted the data to the Langmuir model (Eq. 2.7). Specific adsorption was calculated using eq. 2.1 and vertical error bars were calculated by error propagation. See Appendix D for more information on values and errors obtained.

Table 3.1 summarizes the obtained parameters from the fits and the reduced χ^2 . For the first and second data sets, the K and m_{max} are within the errors of each other, therefore we considered them to be statistically related, which means we can consider these two data sets as one. When merging the two data sets, we had two equal equilibrium concentration from different samples (P1A and P3B, which have a c_{eq} of 0.02 and P2B and P2A of 0.04) with different specific adsorptions. We averaged the specific adsorption and combined its respective errors.

From the fit of the merged data, we obtained a K value of 23 ± 3 mL/mg and a m_{max} value of 445 ± 10 mg/g and a χ_r^2 of 2.6, which is a satisfactory result. Meissner et al. [19] performed a similar experiment, incorporating Lys into SBA-15 at pH 7 and 100 mM ionic strength and fitted their result to a Langmuir model, as well. They obtained a m_{max} and a K value of 281 mg/g and 18 mL/mg respectively. Our K value is close to their results, but m_{max} is almost 50 % higher as theirs. When comparing these values, we should take into account that they used a slightly smaller pH and much less salt. As mentioned before, the ionic strength, related to the amount of salt, is an important factor, since it increases adsorption [63] and even though, there is only a small pH difference, pH 7.4 is closer to Lys' DT, therefore there is lower electrostatic

repulsion between Lys' molecules [63]. Therefore, it is expected that, because of the conditions under which we performed encapsulation, our adsorption results are higher than Meissner's.

3.2.2 Thermal Analysis of Lys samples

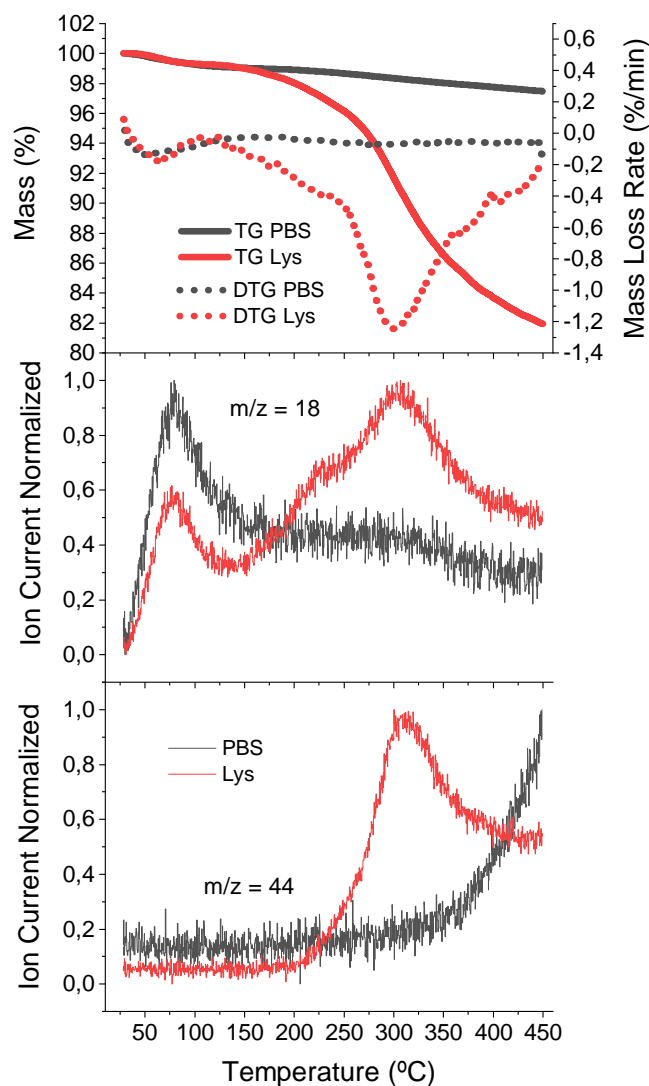


Figure 3.5: TG and MS results for Lys P5A (red) and C (black) , that is Lys + SBA-15 and PBS + SBA-15. The top image shows the TGA (full line) and dTGA results for both samples. Middle and bottom images shows the curves for $m/z = 18$ and 44, respectively.

Fig. 3.5 shows the TGA and MS results at $m/z = 18$ and 44 for a control PBS sample (PBS) and sample P5A. The plots are on top of each, so that the alignment of the peaks are visible. From the TGA results of both samples we can observe a first 0.5 % mass loss, this decrease is accompanied by a peak in the dTGA at $60\text{ }^\circ\text{C}$ and another peak on the water signal at $80\text{ }^\circ\text{C}$. This loss was already identified in the SBA-15 samples and it derives from dehydration. The control sample shows a continuous decrease in mass, due to a continuous loss of more bound water, similar to what was already observed for the SBA-15 case. The Lys sample, on the other hand, shows an abrupt mass loss of 18 % starting at $200\text{ }^\circ\text{C}$: in this case, the water loss is accompanied by protein degradation, as we can observe for the increase of MS at $m/z 44$, starting, also, at $200\text{ }^\circ\text{C}$. The existent peaks at $300\text{ }^\circ\text{C}$ from the dTGA and MS, which are not present for the control sample, are a clear sign of protein presence in the sample.

Fig. 3.7 shows the FTIR of the same Lys P5A sample. From the FTIR we are able to observe different bands that were not present in the SBA-15+PBS spectrum (Fig. 3.6): a double sharp peak at 930 and 960 cm^{-1} due to ammonia (NH_3), a broad peak at $2900 - 3020\text{ cm}^{-1}$ attributed to CH stretching and double broad peak at $3200 - 3400\text{ cm}^{-1}$ due to NH stretching. As Lys is formed by many aminoacids, these bands are a sign of protein presence in the sample [64].

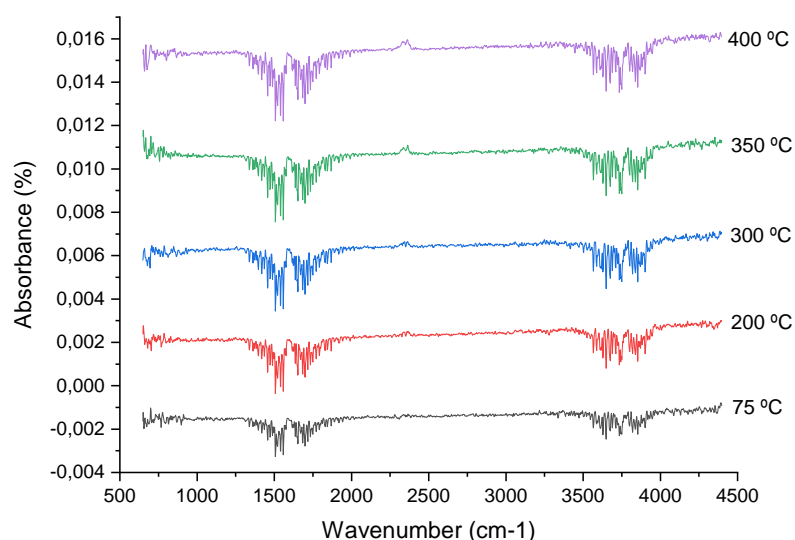


Figure 3.6: FT-IR of PBS + SBA-15 (control for Lys samples) for temperatures: $75\text{ }^\circ\text{C}$ (black), $200\text{ }^\circ\text{C}$ (red), $300\text{ }^\circ\text{C}$ (blue), $350\text{ }^\circ\text{C}$ (green) and $400\text{ }^\circ\text{C}$ (purple).

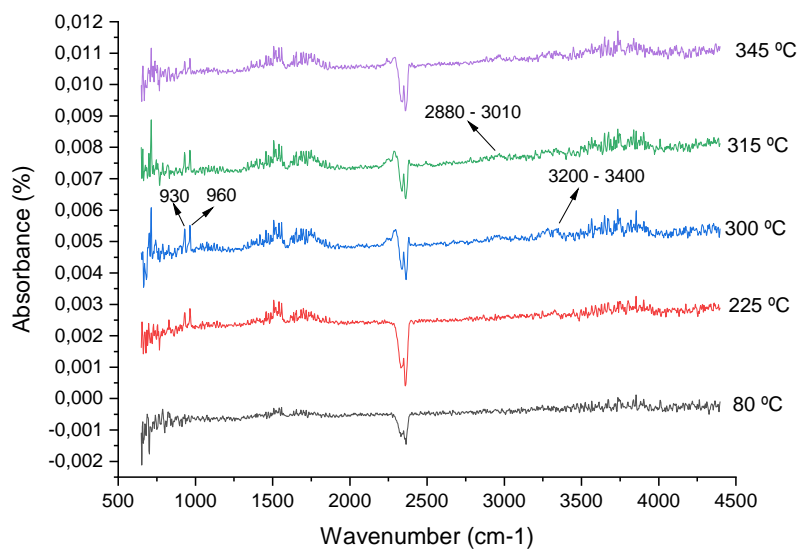


Figure 3.7: FT-IR of SBA + Lys for temperatures: 80 °C (black), 225 °C (red), 300 °C (blue), 315 °C (green) and 345 °C (purple). Vibrations at 930 and 960 and at ranges 2880 – 3010 and 3200 – 3400 cm^{-1} are highlighted.

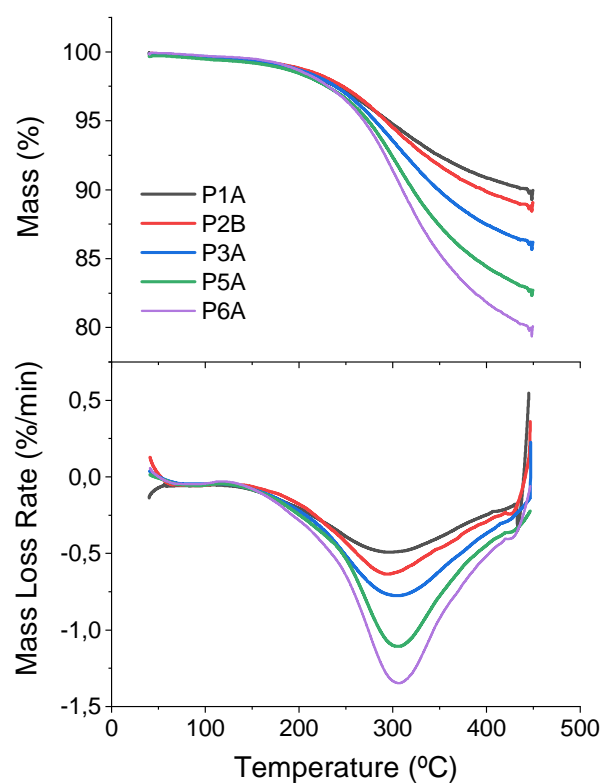


Figure 3.8: Figure on top shows the TGA curves of the samples with different concentrations and figure on the bottom the dTGA. Black, red, blue, green and purple corresponds to samples P1A, P2B, P3A, P5A and P6A, respectively.

We performed TGA for samples with different concentrations, in order to compare the protein adsorption with the UV-Vis results. The results are represented in Fig. 3.8. The TGA curves follow the same trend and the total mass loss per sample increases from point P1 to P6 (Table 3.2). Taking a closer look into the dTGA results, there is a slight shift in temperature peak minima (T_{minima}) from P1A and P2B to P3,5 and 6A (Table 3.2). The shape of the curves is not completely the same, either. In order to better observe these differences, Fig. 3.9 shows the normalized MS at m/z 18 and 44 for the samples with extreme concentrations: P1A and P6A. There is a clear difference in shape for both curves. For the other samples, its behaviour ranges from the P1A to P6A, according to its concentrations (see Appendix C). We hypothesize that, depending on protein concentration, protein and water are distributed differently for these samples [26]. The individual MS and FTIR of these samples can be visualized in Appendix C.

Through UV-Vis, we can calculate the protein mass in each sample and therefore its protein %. Since we did not fully degrade the protein, we cannot compare directly these values with the TGA values for mass loss, but we can compare the order (from lower to highest %) and the UV-Vis and TGA order should match. The protein % present in each sample is calculated, from the UV-Vis measurements, as:

$$protein\% = \frac{m_{protein}}{m_{protein} + m_{SBA-15}} \quad (3.1)$$

Table 3.2 shows the protein % calculated through UV-Vis and the percentual mass loss calculated by TGA and dTGA measurements. As expected, the one that shows the higher protein % also shows a higher mass loss and the sample order, from highest to lowest protein %, calculated by UV-Vis matches the TGA order. Based on these findings, we can conclude that the trends observed in the wet and dry samples seem to match and that a clear dependence between protein concentration and incorporation behaviour occurs.

Table 3.2: Table of protein % for each sample, calculated by UV-Vis (%UV-Vis) and from the TGA (% TGA).

Sample	% UV-Vis (%)	% TGA (%)	T_{minima} (°C)
P1A	14.8 ± 0.9	9.7 ± 0.5	298
P2B	17.2 ± 1.2	10.9 ± 0.4	292
P3A	22.0 ± 1.8	13.5 ± 0.3	304
P5A	25.0 ± 1.1	16.9 ± 0.5	303
P6A	29.0 ± 1.0	19.6 ± 0.2	305

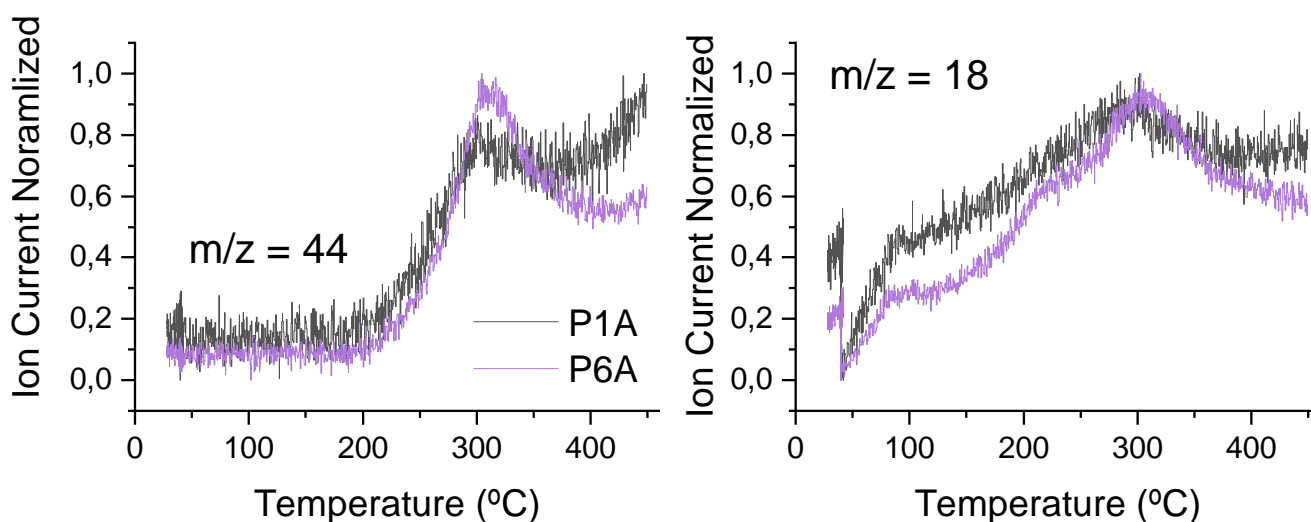


Figure 3.9: Left: MS at $m/z = 44$ of samples P1A (black) and P6A (purple. Right: MS at $m/z = 18$ of samples P1A (black) and P6A (purple.)

3.3 Characterization of Control Samples

We did 3 different measurements of the control samples: CA and CB (first and second set) from room temperature to 450 °C and a third measurement of the CB samples until 1050 °C. For simplicity, let us label these measurements as CA450, CB450 and CB1050. For each pH, these 3 measurements should show approximately the same results. Figure 3.10 shows the mentioned results: for pHs 5.6 and 7.4, the results display the same overall behaviour, despite showing differences, but for pHs 2.9 and 9.1, the thermal decomposition path is not the same between all 3 samples. Therefore, we hypothesize that the salt distribution is not homogeneous for any pH, but especially for pHs 2.9 and 9.1. Previous results have already shown that for PBS buffer in SBA-15, the salts

were not distributed homogeneously [26]. Appendix G shows a table with the different mass samples, for all measurements.

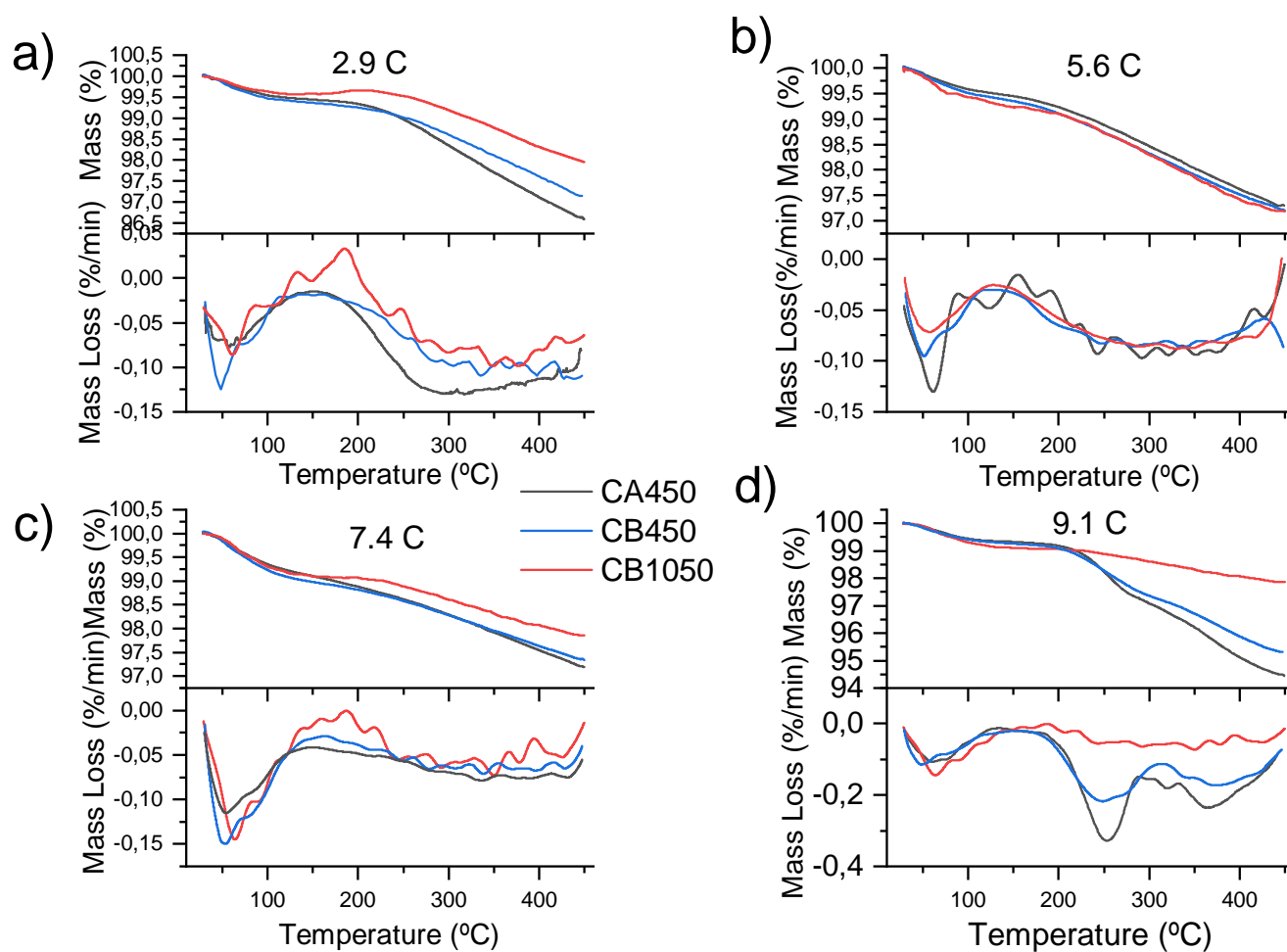


Figure 3.10: Comparison of TGA (top) and dTGA (bottom) results of controls samples (CA450, CB450 and CB1050) for: a)pH 2.9, b)pH 5.6, c)pH 7.4 and d)pH 9.1.

The next step was to compare the thermal profile of the control samples for each pH, in order to identify any differences between them. Figure 3.11 shows the TGA and dTGA results for the CB1050 samples for different pHs and SBA-15 sample measured until 1050 °C, as well. From the TGA, we can observe that each sample is losing mass at a different way. Taking a better look at the dTGA curves all samples have the first initial peak at approximately 65 °C, that has already been assigned to dehydration, but for 7.4C and 9.1C, it seems that these peak have a prolonged tail on the right side, which means that these samples lose surface water at a slower pace than the others. After, there is a continuous loss of more bound water from 200 to 600 °C, that it is also common

to all samples, except for 9.1C, for which this mass loss happens with a two step process. From 600 until 1050 °C, there is a clear difference between the SBA-15 and control samples: while the SBA-15 shows a flat line until the end of the measurement, the control samples show a peak at approximately 820 °C, therefore these peaks are a sign of salts presence inside the SBA-15's pores. For different pHs, this peak has different intensities and it can be slightly shifted, depending on the amount of salts present on the sample and how tightly bound they are, respectively. Table 3.3 summarizes this information. pHs 5.6 and 9.1 show a higher mass loss than pHs 2.9 and 7.4 : possibly the buffer salts in the latter samples have a more attractive interaction with SBA-15, than the salts from the previous pHs, since it requires more energy for the salts to be released.

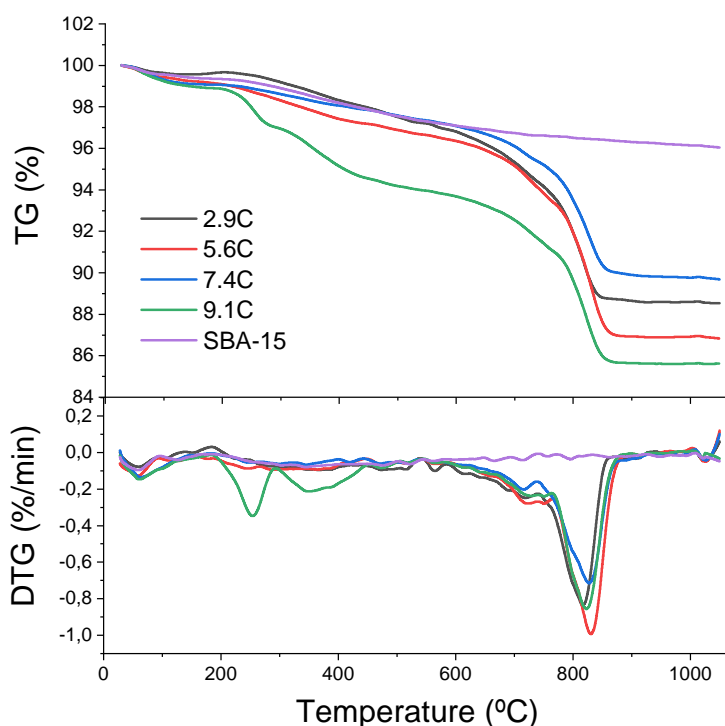


Figure 3.11: TGA (top) and dTGA (bottom) results of controls samples CB1050 for all pHs and SBA-15.

Fig. 3.12 shows the $m/z = 18$ profile from the MS measurements. The curves were normalized, since the focus is the difference in shape of the curves and not the intensity, and smoothed, to facilitate the comparison between each sample. As expected the $m/z = 18$ profile appears to be different for all samples. Therefore, the samples are losing water, and consequently mass, at

Table 3.3: Table summarizing, for each CB1050 sample overall mass loss, area under peak and T_{peak} .

Sample	Overall Mass Loss (%)	Area under curve (%)	T_{peak} (°C)
2.9C	11.5	5.7	816
5.6C	13.2	6.8	830
7.4C	10.3	5.6	828
9.1C	14.4	5.5	823

different trends, which can be observed by the different steps and temperatures associated to each step. The thermal decomposition path and water dynamics is different between all samples, therefore we hypothesize that the pH and/or acids present in the buffer composition affect the salt distribution inside the SBA-15 [65, 66]. This means that the environment under which we are performing DT incorporation is not the same throughout all samples, which affects the diffusion pattern and therefore distribution of protein inside the SBA-15.

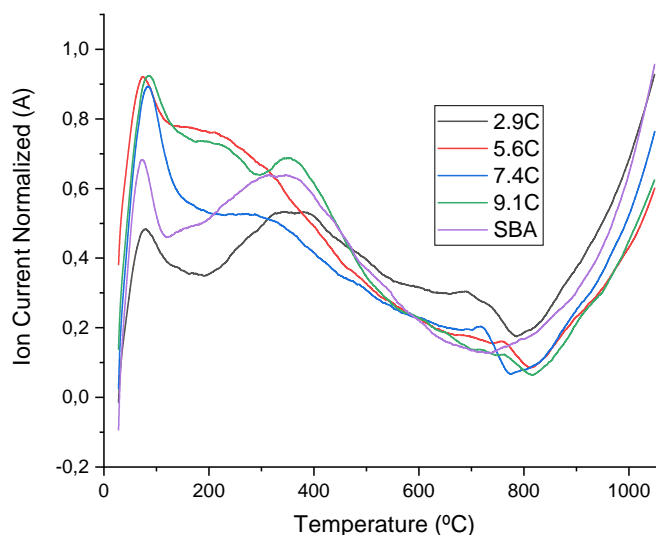


Figure 3.12: MS results of the $m/z = 18$ (H_2O) profile for controls samples CB1050 for all pHs and SBA-15. The curves were smoothed and normalized.

3.4 DT results

3.4.1 DT adsorption into SBA-15

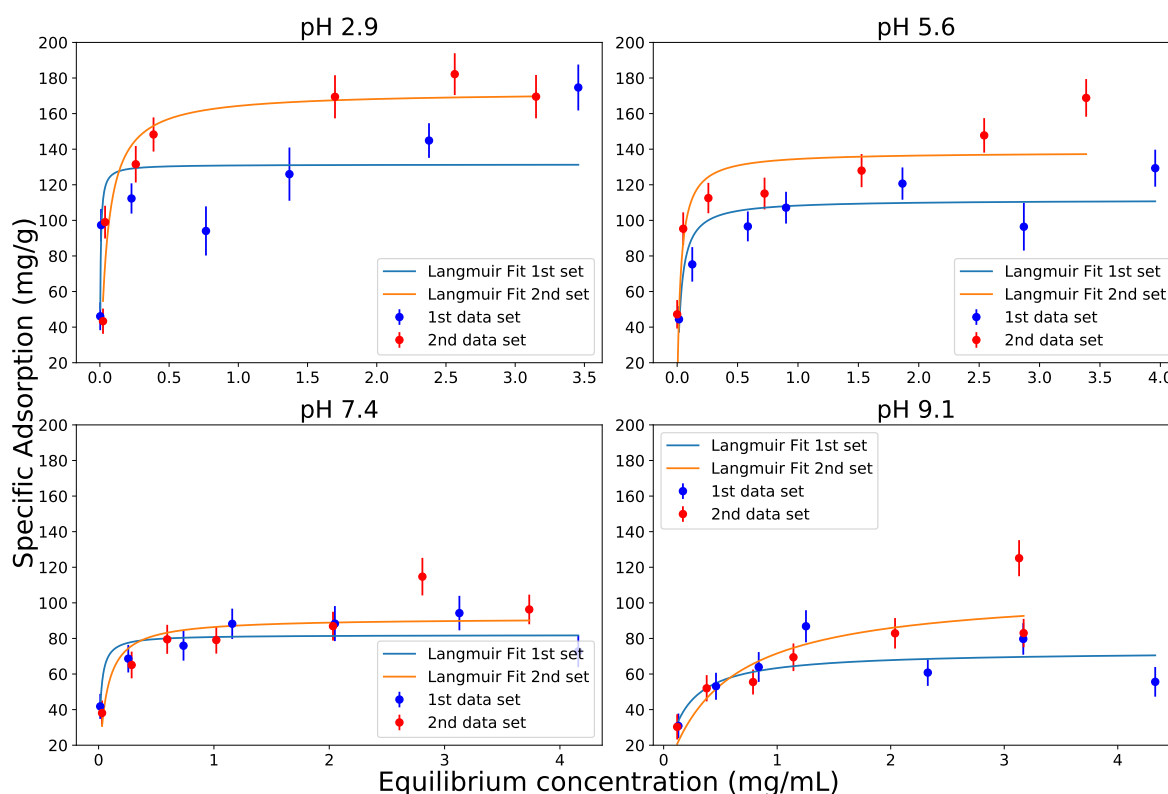


Figure 3.13: Isotherm of DT into SBA-15 at different pH for first and second set (red points) of samples and respective Langmuir fits for : pH 2.9 (upper left), pH 5.6 (upper right), pH 7.4 (bottom left) and pH 9.1 (bottom right). Points represents datapoints (blue for first and red for second data set), vertical line represents the error on the y-axis and solid lines correspond to the Langmuir fit (blue for first and yellow for second data sets).

We performed DT incorporation into SBA-15 for 4 different pH's: 2.9, 5.6, 7.4 and 9.1 for the first and second set of samples. We plotted an adsorption isotherm for each pH series and fitted the results to a Langmuir model. The plots are shown in Fig. 3.13 and the parameters of the fits are summarized in table 3.4. For a better understanding of the shapes of the fits, see Appendix E and for experimental values obtained, see Appendix F.

Table 3.4: Results for the Langmuir fit for DT incorporation into SBA-15 for pH 2.9, 5.6, 7.4, 9.1 first and second data set (reduced χ^2 , parameters and respective errors).

		K	m_{max}	χ_r^2
2.9	1st set	246 ± 54	131 ± 5	5
	2nd set	21 ± 3	172 ± 6	2.5
5.6	1st set	34 ± 10	112 ± 5	2.1
	2nd set	35 ± 11	138 ± 5	10.5
7.4	1st set	68 ± 25	82 ± 4	1.1
	2nd set	17 ± 6	92 ± 3	2.1
9.1	1st set	7 ± 3	73 ± 5	2.3
	2nd set	2.0 ± 0.6	107 ± 9	3.4

As expected, from the difference between control samples, the shapes of the fit curves are different for each pH series, but unexpectedly, it is also different within the same pH (between 1st and 2nd sets). Some of the data points do not seem to plateau, but instead portray a continuous increase (pH 2.9 1st and 2nd set, pH 5.6 2nd set and pH 9.1 2nd set), which is not similar to a Langmuir model. Nevertheless, as a first approach, the Langmuir model is the most simple and common model to describe protein's adsorption into SBA-15, which allows us to treat each pH series equally and perform direct comparisons between pH series. Taking a closer look at the parameters given by the plots from table 3.4, K and m_{max} values for matching pH series (first and second sets) are very different and are not within the confidence interval of each other, except for the K value of pH 5.6. As expected, the χ_r^2 values also do not match between first and second data set for each pH series. There is a tendency for higher m_{max} and lower K values for the second set, that is higher adsorption levels and lower affinity between SBA-15 and DT. Opposite to the Lys case, we did not merge the first and second data set as one, since it is safer to assume that they are not the same, since they are statistically different. Therefore, we did not consider the second data set as duplicates of the first and considered each data set individually.

The second data set stems from the second set of samples, which were not fully created under the same initial conditions as the first set of samples, but under the assumption that we could mimic those conditions by reusing the protein. We can, therefore, hypothesize that this process is not optimal, since it does not lead to similar results. That is possibly due to the effect of pH on the protein and possible changes in its structure. As we observed from the control

sample characterization, each sample had a different decomposition paths, consequently the conditions under which the incorporation is performed is different and that might affect the protein. For example, the higher adsorption and lower affinity for the second set samples could possibly be caused by protein aggregation that happened throughout protein incorporation of the 1st set samples.

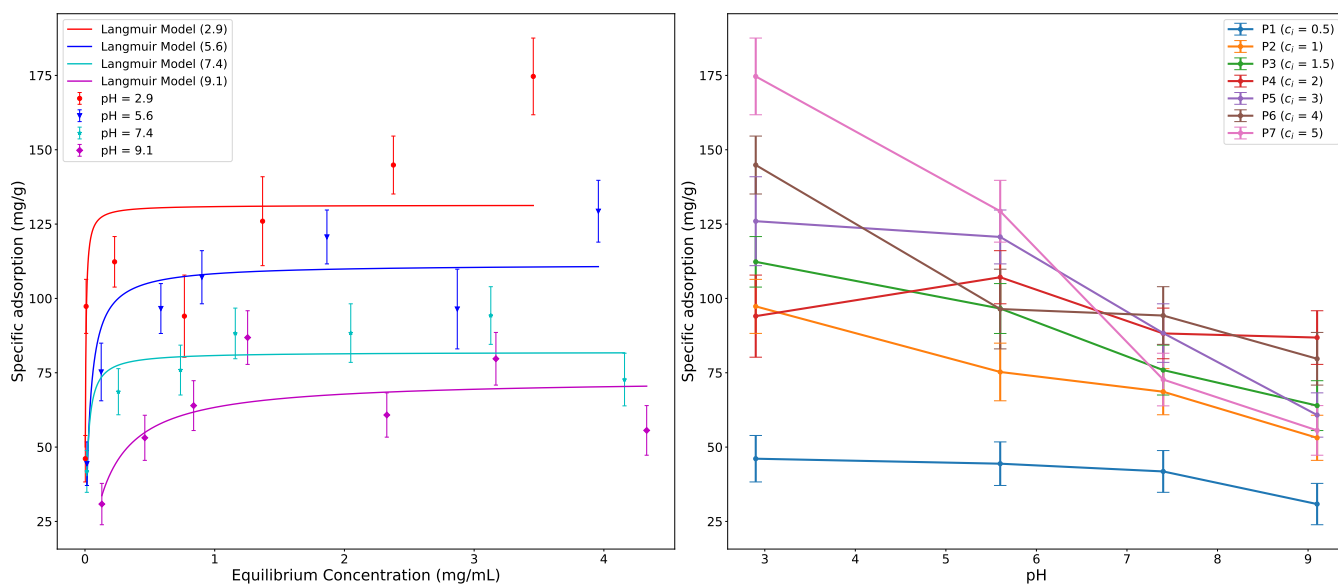


Figure 3.14: Left plot shows an isotherm of DT into SBA-15 at each pH for the first set of samples: pH 2.9 (red), pH 5.6 (red), pH 7.4 (cyan) and pH 9.1 (magenta). Right plot shows specific adsorption as a function of pH: each color represents a data set with the same initial DT concentration used for incorporation. For both plots, points represents datapoints (blue for first and red for second data set), vertical line represents the error on the y-axis and solid lines correspond to the Langmuir fit.

Focusing on the first data set curves: for pHs 5.6, 7.4 and 9.1, the reduced χ_r^2 is close 1. For pH 2.9, χ_r^2 and K values are too high and we considered the model does not fit the data. For pH 9.1 series, even though the χ_r^2 is satisfactory, the K value is very low and its shape does not resemble a Langmuir function, since it does not show a fast increase for low concentrations. Thus, we consider the model fits the data satisfactorily well, only for pHs 5.6 and 7.4.

Comparing pH 7.4 with previous Lys results, we have much lower m_{max} values for DT incorporation. At this pH, Lys and SBA-15 are oppositely charged, which facilitates adsorption, while DT and SBA-15 are both negatively charged

and since Lys' dimensions are much smaller than DT's, the protein can more easily fit into SBA-15's mesopores. Therefore, these results are following our expectations. The order from highest to lowest m_{max} value for each pH series is: $2.9 > 5.6 > 7.4 > 9.1$, thus specific adsorption decreases with pH. Nevertheless, this tendency is not followed for every initial concentration used during incorporation. The right plot on Fig. 3.14 shows specific adsorption as a function of pH, therefore each colourful curve represents a different concentration series (different pH and same initial concentration). For P4 samples ($c_i = 2$ mg/mL) there is a different trend than for all the other concentration series: there is an increase in adsorption from pH 2.9 to pH 5.6, instead of a decrease.

3.4.2 Thermal Analysis of DT samples

Figs. 3.15 and 3.16 show the TGA and dTGA curves stacked on top of the MS at $m/z = 18$ and 44 for samples P5A and respective control sample for pH 2.9, 5.6, 7.4 and 9.1. The curves are stacked on top of the each other, so that it is easier to understand the correlation between plots: each peak in the dTGA curve is perfectly aligned with the peaks in the MS.

Each TGA curve for the DT samples, independent of the pH, shows 3 mass loss steps; these steps can be better visualized through the peaks in the respective dTGA curves. For the control samples, the second step is still existent but much more subtle, therefore, there is a clear protein presence in the DT sample. The first and second steps of the control samples, similarly to PBS control, is attributed to dehydration and loss of bound water, respectively. For the DT samples, the first mass loss is, again, due to dehydration, but the second step is mainly due to protein degradation, along with loss of bound water. This bound water is not fully the same as in the control case: it refers to both the mentioned water in the control case and water trapped in the protein structure - during the heating process the protein is decomposed and releases water molecules. Finally, the third peak is present in both control and DT samples and its shape is similar but shifted to higher temperatures for the DT samples. This step is mainly due to loss of OH- group in surface silanols, but in the DT case, there is still protein loss happening at these higher temperatures. Table 3.5 summarizes the temperature and mass loss associated to each mass loss step. The second mass loss step for the DT sample for pH 9.1 is in fact two

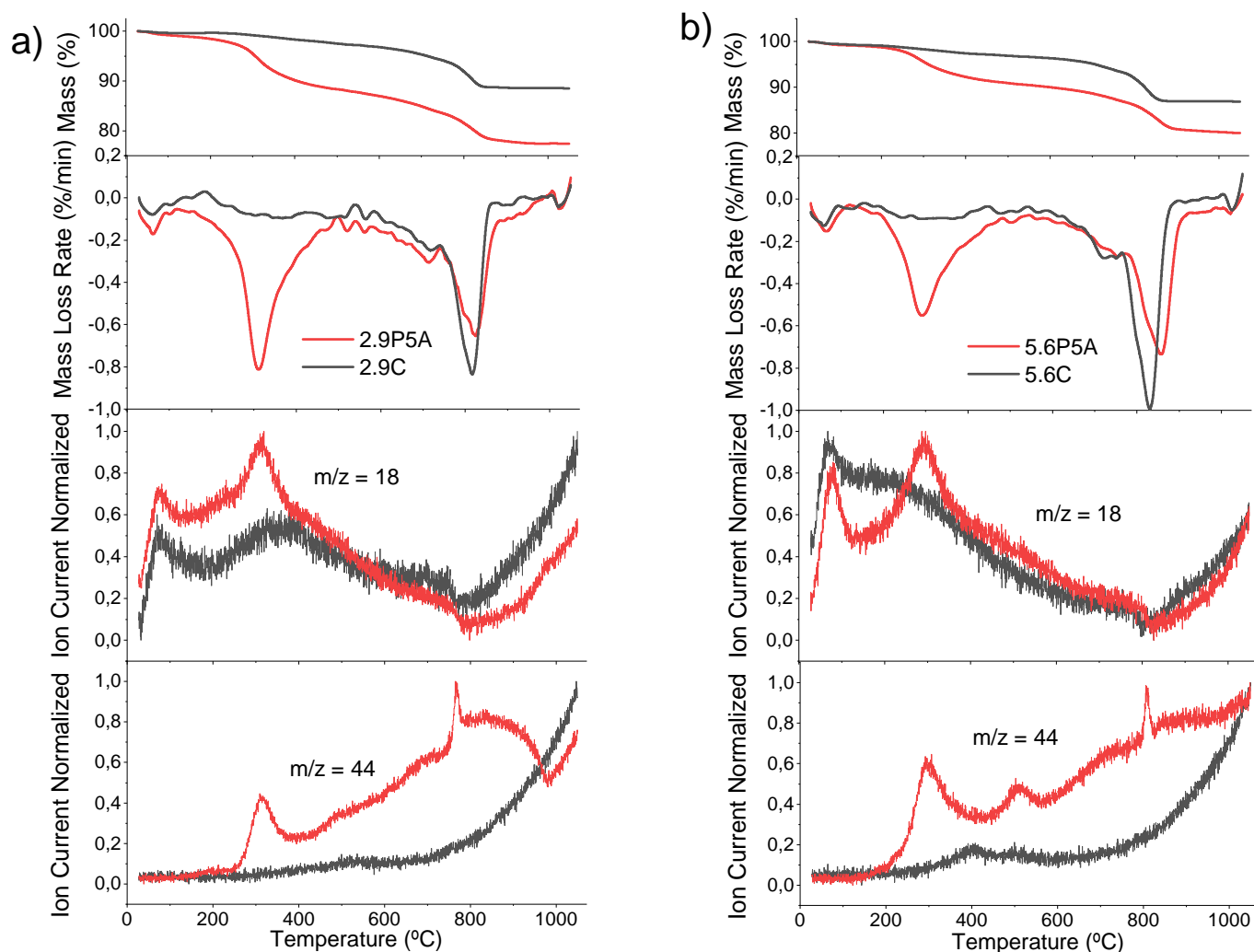


Figure 3.15: Comparison of TGA and MS at $m/z = 18$ and 44 results of P5A and the control sample associated to the pH series in question for pH: a) 2.9 and b) 5.6.

steps happening in one, it is more complex than the others and it is not a single peak, therefore we cannot distinguish the peak's temperature. The mass loss associated to each step was calculated from the area below each dTGA curve.

The material assigned to each TGA mass loss step can be better understood by a closer analysis of the MS curves:

- 1st Mass Loss Step

The first peak in the TGA, both for the DT and control samples, is perfectly aligned with the first peak in the water signal ($m/z = 18$). This

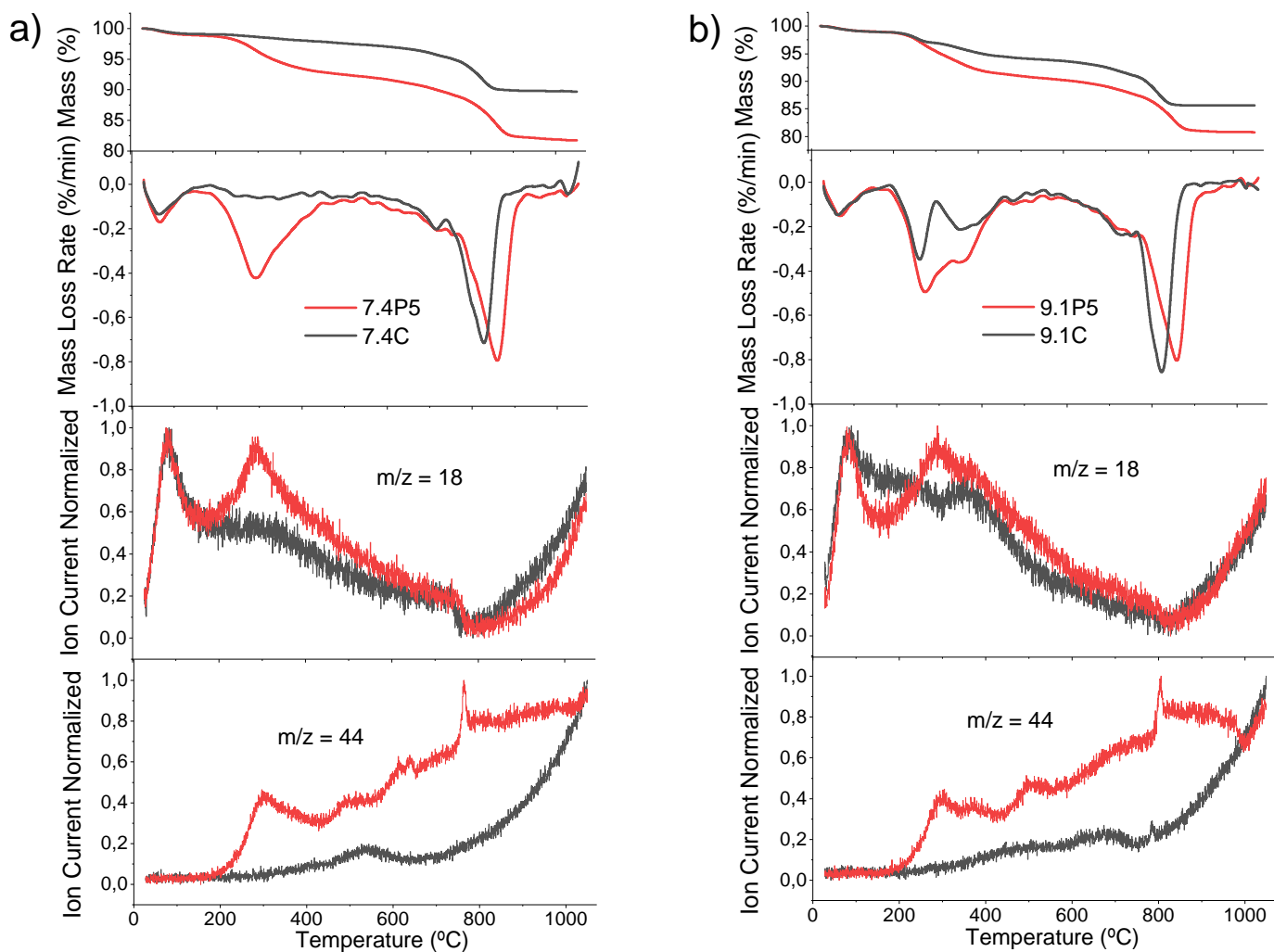


Figure 3.16: Comparison of TGA and MS at $m/z = 18$ and 44 results of P5A and the control sample associated to the pH series in question for pH: a) 7.4 and b) 9.1.

peak has been present throughout all the samples we have studied and corresponds to loss of surface water.

- 2nd Mass Loss Step

For the control samples, this is a continuous mass loss step, which translates into a low intensity, but large dip in the dTGA curves. For different pHs, the $m/z = 18$ shape is different right after the first peak, but nevertheless shows high values, symbolizing the water presence. For the control case, the $m/z = 44$ signal stays low, except for the impurity peak, that is already present in the SBA-15 sample. For the DT case, there is a prominent second peak in the dTGA, accompanied by a clear

peak at the same temperature in the $m/z = 18$ and followed by smaller peak(s) in the $m/z = 44$.

- 3rd Mass Loss Step

This step was already present in the SBA-15 samples. For the control samples, both the $m/z = 18$ and 44 are very similar to SBA-15's profile: an abrupt increase from a low to high signal for both m/z 's. Right at the start of this step, there is a quick decrease in the water signal, for control and DT samples. Simultaneously, there is a sharp peak for the DT's $m/z = 44$, followed by a stable signal until it overlaps with the control's signal (temperature at which all protein has been degraded). We hypothesized that the sharp peak is due to the presence of extremely bound protein attached to the surface silanols: when the OH bound of the silanols break, then the protein bond breaks as well - this step happens very abruptly and exposes more protein that was protected by the SBA-15's structure.

Table 3.5: Temperature and mass loss associated to each step in the TGA curve (Figs. 3.15 and 3.16) for control and DT samples. T1, T2 and T3 refer to the temperature of the dTGA peak associated to 1st, 2nd and 3rd step respectively and ML1, 2 and 3 to the mass loss of each step, calculated by the area under the dTGA curve.

	T1 (°C)	ML1 (%)	T2 (°C)	ML2 (%)	T3 (°C)	ML3 (%)
2.9C	60	0.3	—	2.0	810	6.0
2.9P5A	60	0.8	310	10.0	820	6.0
5.6C	62	0.6	—	2.0	830	7.0
5.6P5A	66	0.8	290	8.0	860	7.0
7.4C	64	0.9	—	1.0	827	6.0
7.4P5A	68	1.0	291	6.0	858	8.0
9.1C	61	1.0	—	4.0	820	5.0
9.1P5A	68	1.0	?	8.0	858	7.0

From comparison of Figs. 3.15 and 3.16, we can observe big difference in the thermal degradation processes for different steps. Let us now take a closer look into those differences: Figs. 3.17 and 3.18 show the TGA and MS at $m/z = 18$ and 44 results for the same DT samples (2.9P5A, 5.6P5A, 7.4P5A and 9.1P5A). the curves shown have been normalized and smoothed. Appendix G shows a table with the sample's mass.

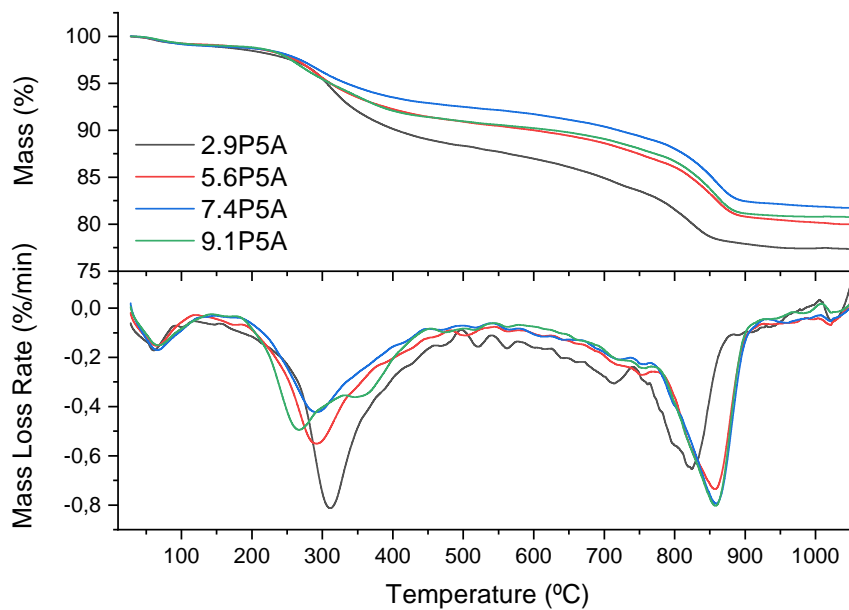


Figure 3.17: Comparison of TGA results of P5A for pH 2.9, 5.6, 7.4 and 9.1.

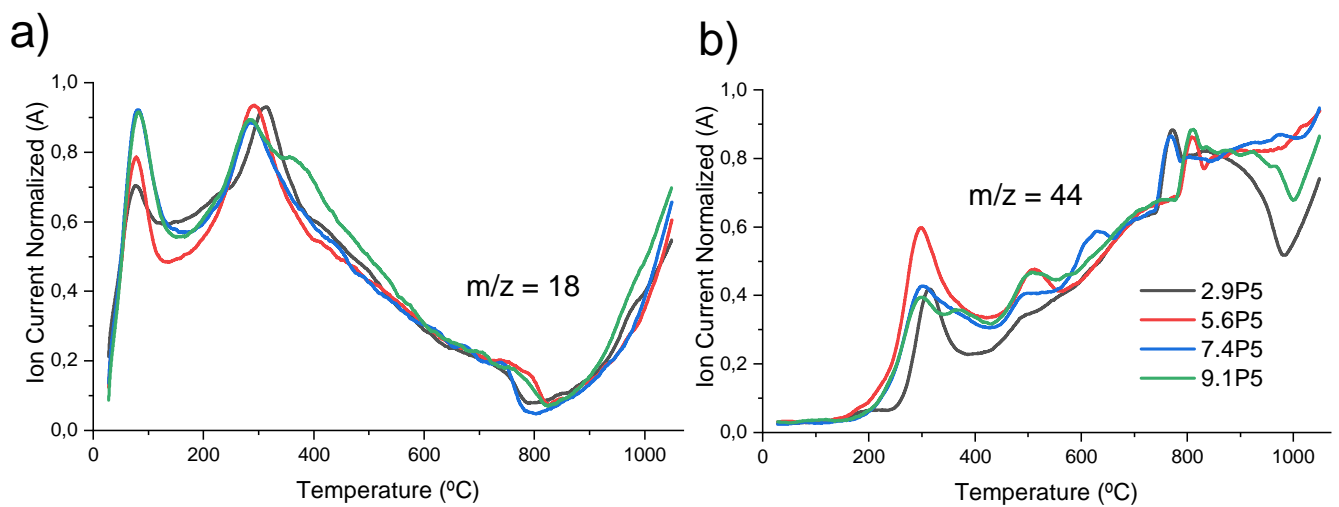


Figure 3.18: Comparison of MS at $m/z = 18$ and 44 results of P5A for pH 2.9, 5.6, 7.4 and 9.1.

For all samples, the TGA steps' shape looks similar, except for the height of each step and the starting temperature of the step (Fig. 3.17). These differences are also observable in the dTGA curves by the horizontal shift and intensity of each peak (Table 3.5). As we have mentioned for previous analysis, this is related to the amount of protein present in the sample and how attached

it is to the SBA-15 structure. The first is already to be expected since each sample has different protein %s (% UV-Vis Table 3.6a). For pH 9.1, there is a clear difference in the shape of the second dTGA peak: as we have mentioned before, there are two steps happening roughly at the same time, between 200 and 450 °C. From these curves, we can already deduce that the thermal decomposition path is different between samples, but it becomes even more clear by analyzing the MS curves. From the water profile (Fig. 3.18a), we can observe that, for every sample, there are 3 water species (surface, bound and very bound water). Each sample releases surface and very bound water similarly (there is only a difference in intensity for surface water), but not bound water: between 200 and 800 °C, the shape and intensity of the curves is different, therefore the water is distributed differently, depending on pH. For the CO_2 profile (Fig. 3.18b), the shapes are completely different throughout the whole temperature range. These shapes become more complex (more peaks), the higher the pH: this is a sign that the protein is not degrading in one simple step, but in a multiplex trend. Possibly, the protein is not distributed uniformly throughout the SBA-15 and/or is bound differently to the SBA-15 structure and the higher the pH, the less uniform this distribution is or the more protein species (differentiated by how attached they are) it has.

Table 3.6: Protein % present in each sample calculated through UV-Vis (%UV-Vis) and TGA measurements (%TGA) (a) and temperature at which protein degradation starts (T_{deg}) for each pH (b).

(a)

Sample	%UV-vis (%)	%TGA (%)
2.9P5A	11.2 ± 1.2	10.4 ± 0.4
5.6P5A	10.8 ± 0.7	6.5 ± 0.6
7.4P5A	8.1 ± 0.8	7.7 ± 0.5
9.1P5A	5.7 ± 0.7	4.8 ± 0.2

(b)

pH	Tdeg (°C)
2.9	120 ± 8
5.6	143 ± 11
7.4	159 ± 15
9.1	183 ± 10

Table 3.6a) shows a comparison between the protein percentage existent in each sample, based on a UV-Vis and TGA analysis and 3.6b) the temperature at which protein degradation starts, for each pH. % UV-Vis is calculated using eqn.3.1. % TGA is calculated as previously described in the materials and methods section: for the TGA we considered the difference between the overall mass loss of the sample with DT and the control sample, while for the dTGA we consider the difference between the area below the second and third curves of the dTGA of the DT and control sample. T_{deg} was defined as the temperature at which MS at $m/z = 44$ of the control and DT samples diverge from each

other. To do so, we normalized and smoothed the curves and considered the measurements of samples P5A, P4A and P2A.

For pH 2.9, 7.4 and 9.1, % TGA and % UV-Vis values are within the confidence interval of each other. The same does not happen for pH 5.6. A plausible explanation for this discrepancy is that, based on the approach taken for protein % estimation from dry samples (% TGA), there could have been an over-subtraction of the mass loss of control sample. Possibly, there is a higher mass loss in the control samples, than in the DT samples, leading to an underestimation of the protein % in the sample. From table 3.3, we observe that the control sample loses a lot of mass, almost the same as for pH 9.1, mainly due to loss of buffer salts, but from Fig. 3.17, we can observe that it is the sample that loses less mass and, consequently, less protein, but it is not the sample with less protein (%UV-Vis): it is actually one of the samples with more protein. One possibility is that, when adding protein, the salt-protein and SBA-15 interactions could become more favorable than only between salt and SBA-15, which would lead to loss of less protein, since it is more attached, and in consequence also less salts, if these salts are attached to the protein.

Samples 2.9P5A and 9.1P5A are the samples with the highest and lowest protein %, respectively. As for T_{deg} , even though the uncertainties associated to each value are high and there is a little overlap between the values obtained for pH 5.6, 7.4 and 9.1. Overall, T_{deg} increases with pH. We can, therefore, observe a tendency, for higher protein uptake, but earlier degradation for lower pH. This means that we can incorporate more protein, but the protein is less protected for thermal degradation for lower pHs.

To finalize, we performed TGA measurements to compare samples from the first and second sets. With that purpose, we used samples P2 and P4 (A and B). For all pHs, samples P2A and P2B do not show any difference, either for the TGA and the MS (Fig. 3.19). P2 samples have very little protein, which makes it more complicated to spot difference in protein distribution through MS and TGA (for higher protein concentrations, it is easier to spot differences).

For pH 7.4 and 9.1, samples P4A and P4B already show a slight difference in the dTGA curves (Fig. 3.20). For the MS, it appears that the difference between first and second samples increases for higher pHs (Figs. 3.21, 3.22, 3.23 and 3.24), but overall, all samples show the same trends as described

for Figs. 3.16 and 3.17. Samples from the first and second sets show the same thermal degradation profile: their difference lies only on the amount of protein in its constitution. Thus, it makes sense that the difference between samples from first and second set is very similar to the difference between samples with difference protein concentrations (Figs. 3.25 and 3.26). Any difference in intensity signal for superficial water (from room temperature to approximately 150 °C) between P4A and the other samples is due to different sample preparation for measurements and it is already expected: for samples P4A, before placing the sample in the crucible, we smashed the sample with a milestone and pester to make a fine powder with less superficial water, but using this process, a lot of sample is lost. To prevent that, for the other samples, we mixed and smashed the chunks inside the ependorf.

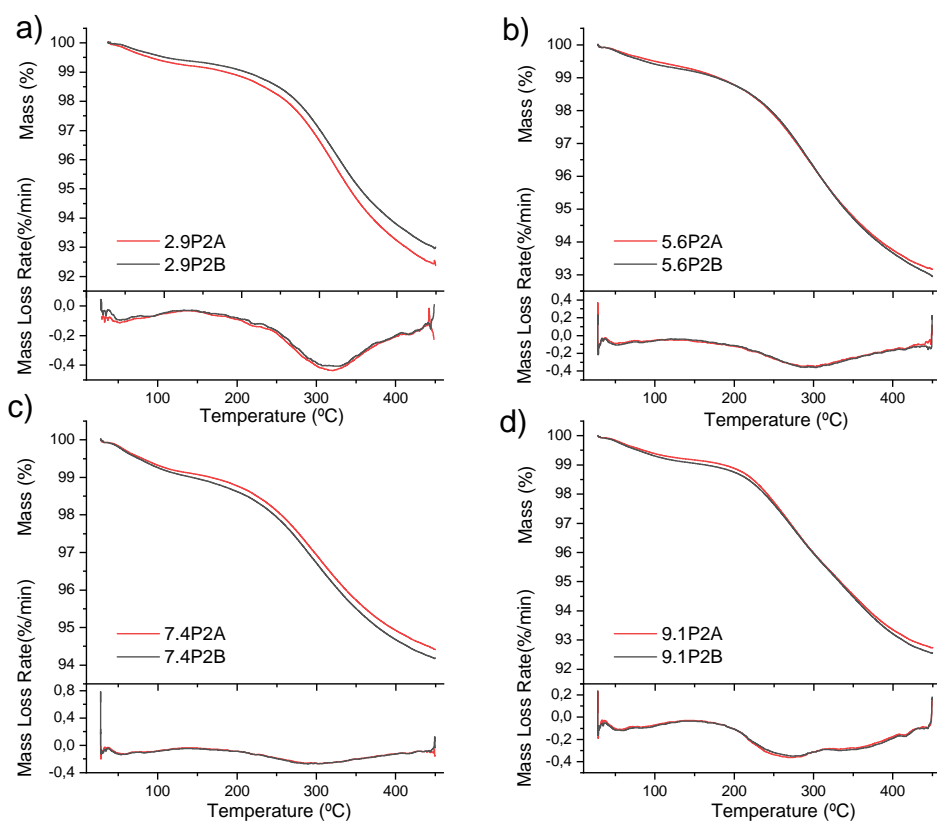


Figure 3.19: Comparison of TGA results of first and second set of DT Samples for pH: a) 2.9, b) 5.6, c) 7.4 and d) 9.1 for P2 ($c_i = 1$ mg/mL).

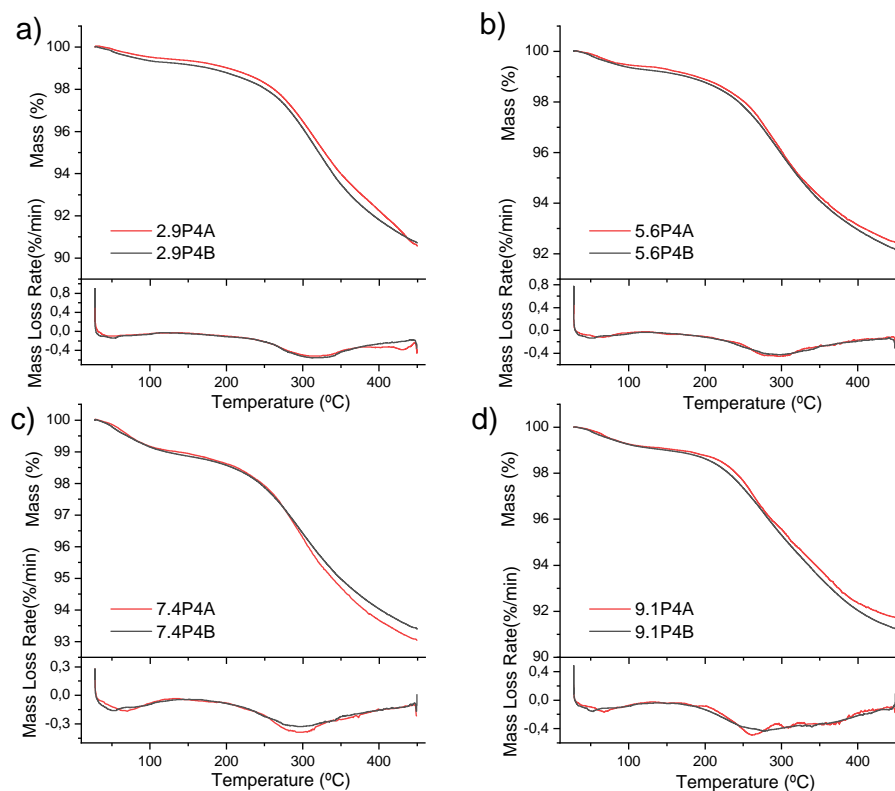


Figure 3.20: Comparison of TGA results of first and second set of DT Samples for pH: a)2.9 , b)5.6 , c)7.4 and d)9.1 for P4 ($c_i = 2$ mg/mL).

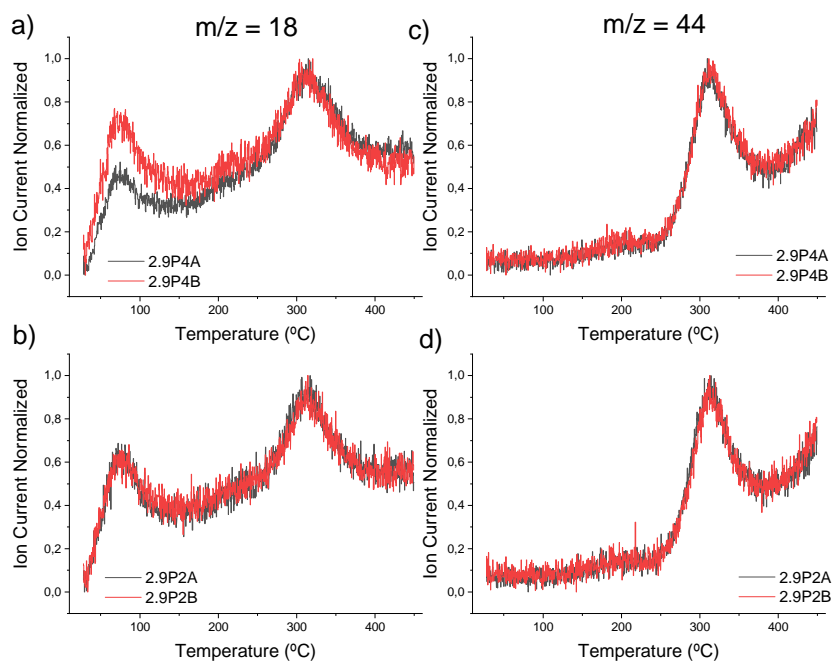


Figure 3.21: Comparison of MS results of first and second set of DT Samples for pH 2.9: a)P4 at $m/z = 18$, b)P2 at $m/z = 18$, c)P4 at $m/z = 44$, d)P2 at $m/z = 44$.

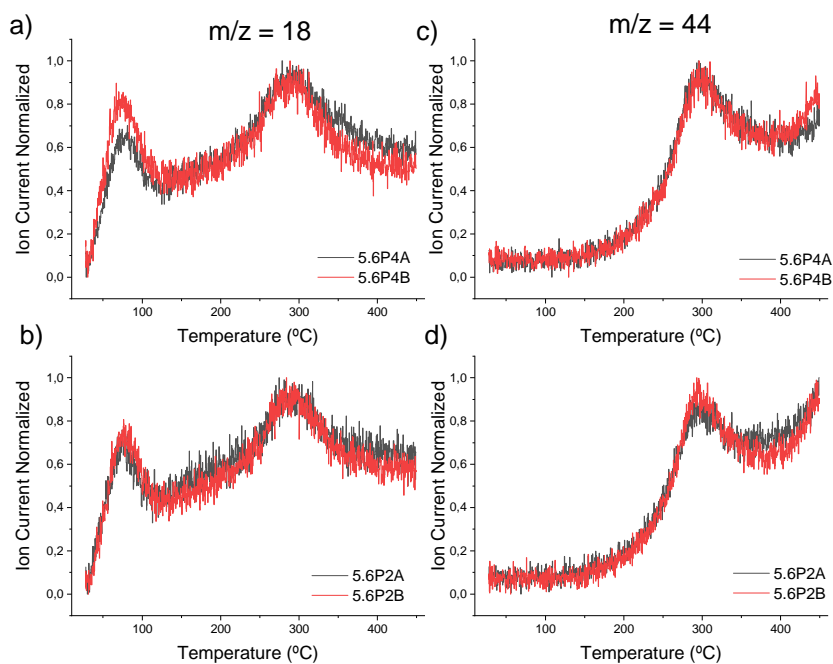


Figure 3.22: Comparison of MS results of first and second set of DT Samples for pH 5.6: a)P4 at $m/z = 18$, b)P2 at $m/z = 18$, c)P4 at $m/z = 44$, d)P2 at $m/z = 44$.

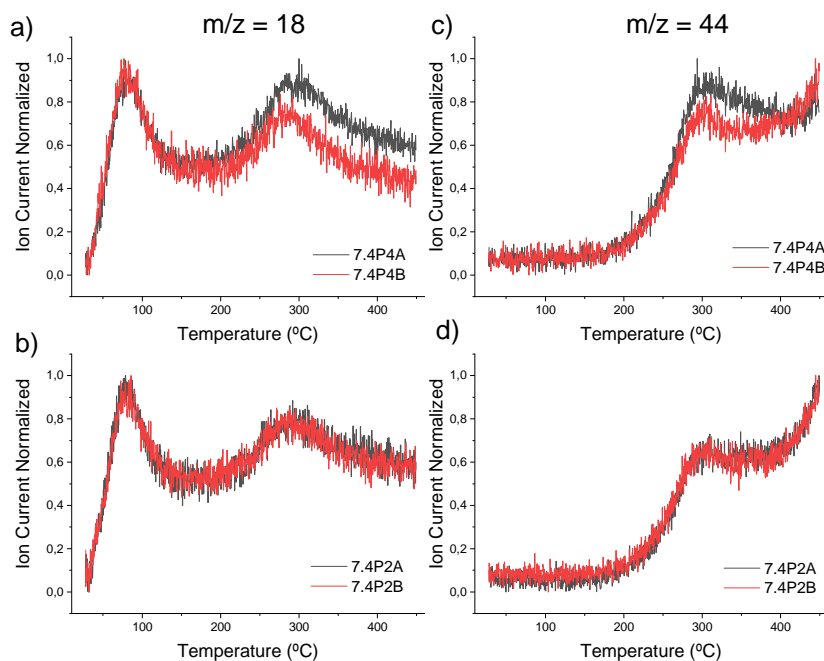


Figure 3.23: Comparison of MS results of first and second set of DT Samples for pH 7.4: a)P4 at $m/z = 18$, b)P2 at $m/z = 18$, c)P4 at $m/z = 44$, d)P2 at $m/z = 44$.

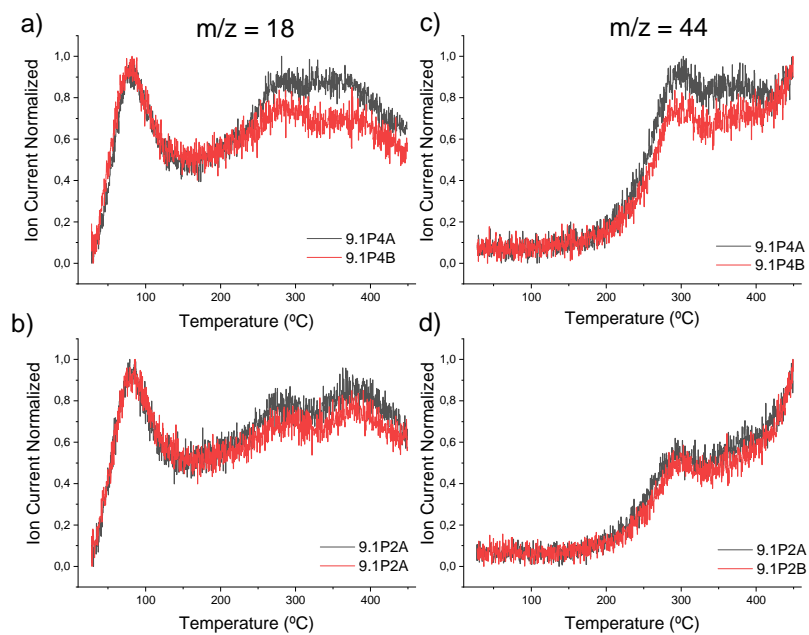


Figure 3.24: Comparison of MS results of first and second set of DT Samples for pH 9.1: a)P4 at $m/z = 18$, b)P2 at $m/z = 18$, c)P4 at $m/z = 44$, d)P2 at $m/z = 44$.

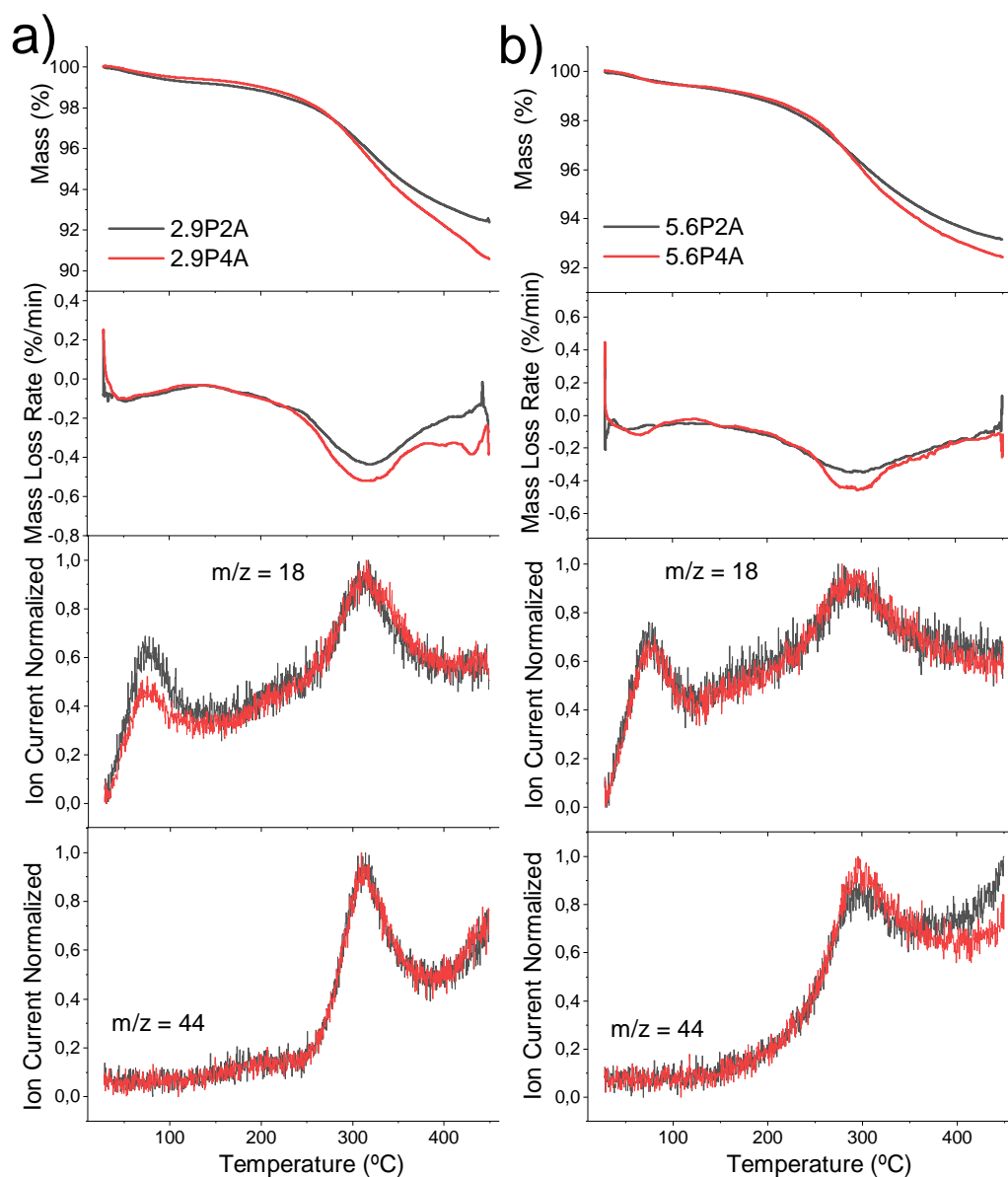


Figure 3.25: Comparison of TGA, dTGA and MS at $m/z = 18$ and 44 results of P2A and P4A for pH a) 2.9 and b) 5.6.

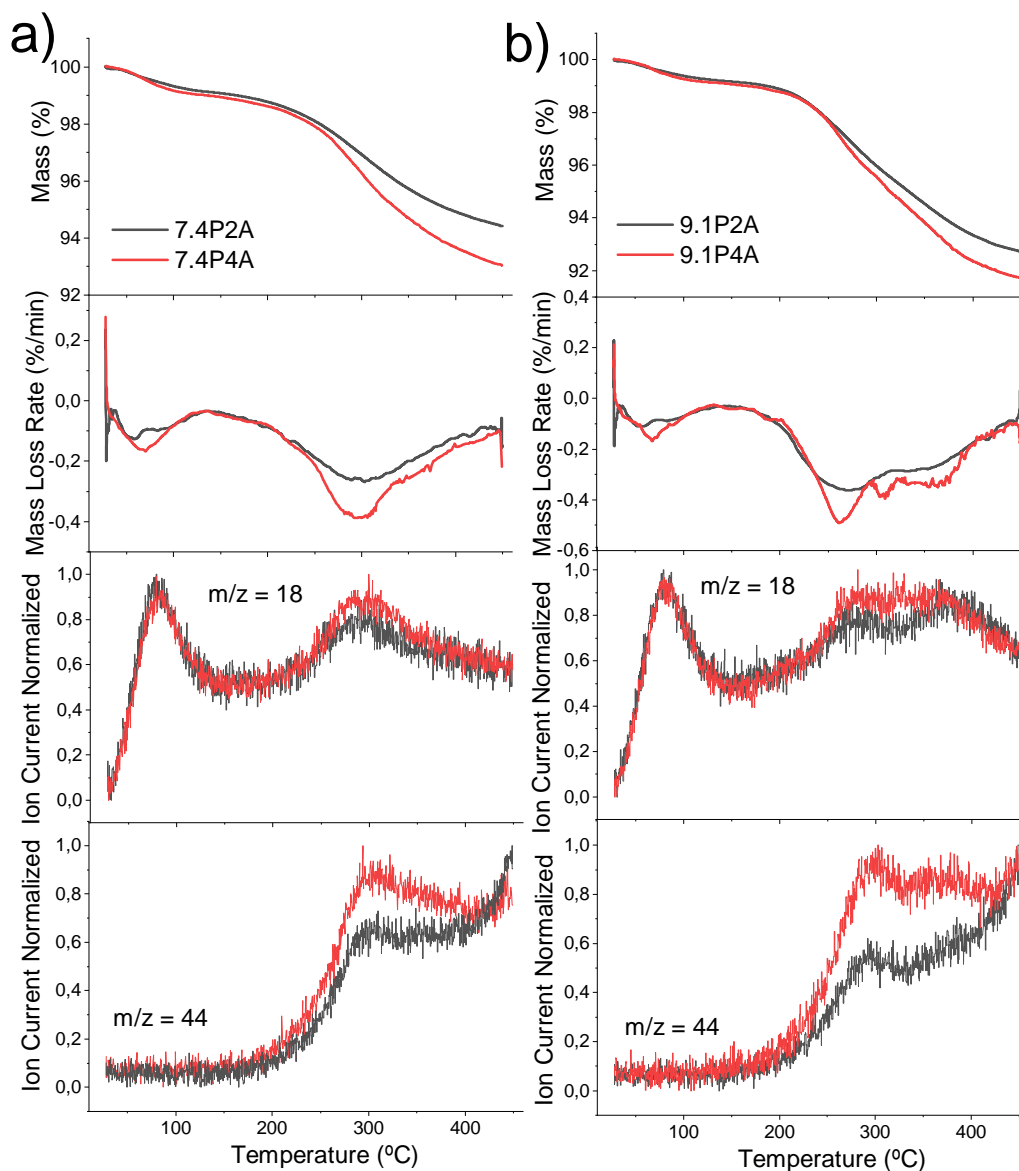


Figure 3.26: Comparison of TGA, dTGA and MS at $m/z = 18$ and 44 results of P2A and P4A for pH a) 7.4 and b) 9.1.

Conclusion

The goal of this thesis was to understand how certain encapsulation conditions, such as pH and protein concentration affect adsorption of DT into SBA-15. We started by characterizing the SBA-15 with TGA-MS-FTIR analysis. The MS and FTIR measurements showed an unexpected release profile of CO_2 , which we attributed to the decomposition of polymer remains from the calcination process used in the material's synthesis [62]. From comparison with different measurements from the same batch of SBA-15, we concluded that the SBA-15 might not be completely homogeneous, meaning that, its pores and leftover impurity are not distributed homogeneously. Nevertheless, it has a good level of homogeneity.

Analysis of the control samples (SBA-15 dispersed in the buffer designed for each pH) showed that, depending on pH, each sample has a different thermal degradation profile and water dynamics (different MS at $m/z = 18$ profiles), which means that the analysis of DT samples becomes more complex, since each pH series is encapsulated under a different environment. These differences could be attributed to pH differences and/or salts presents in each buffer [65, 66]. Possibly the buffer salts of pHs 2.9 and 7.4 have a more attractive interaction with SBA-15 than the salts of pHs 5.6 and 9.1, which would make the control samples for pHs 2.9 and 7.4 more stable.

From the TGA and MS analysis of DT samples, there is a clear protein presence. The samples' thermal degradation profile is constituted by 3 mass loss events: the first one, common to SBA-15 and the control samples, is due to dehydration, the second to protein degradation and loss of bound water and, finally, the third, still shows signs of degradation of very bound protein and loss of OH- from surface silanols. Even though there is a similar overall behaviour, as expected from the difference in control results, the MS and TGA profiles differ between pH series. Based on a detailed analysis of this samples, we hypothesized that proteins are not distributed uniformly throughout the SBA-15 and/or are bound differently to the SBA-15 structure. Interestingly, the

signs of this behaviour (complex thermal degradation and MS profile at $m/z = 44$ profiles) seem to intensify for higher pHs.

From the fitting of the DT isotherm plots of adsorption to the Langmuir model, we observed an uptake increase for lower pHs and pH series 5.6 and 7.4 fitted the model more satisfactorily than for pHs 2.9 and 9.1.

We proceeded to compare the TGA and UV-Vis results, that is, the results based on the measurements of dry and wet samples, respectively. The protein % calculated using UV-Vis spectroscopy matches the values obtained by TGA measurements, where the protein was fully degraded, except for pH 5.6, possibly due to oversubtraction. Therefore, we observed higher protein %, and consequently adsorption, for lower pHs. These results also showed an earlier degradation for lower pHs, which means that DT becomes less thermally protected. From the measurements performed, we concluded that the pH that allows for a higher adsorption is pH 2.9 and the lowest 9.1 and the opposite for thermal protection.

Perspectives

From our analysis, we were able to conclude that the approach used here is very promising to answer what are the most satisfactorily encapsulation conditions, depending on initial concentration and pH.

Based on our results, pH 2.9 seems to be the most satisfactory one, since it allowed for higher adsorption levels. In order to understand if pH 2.9 is indeed the best encapsulation condition, more measurements should be performed. It is important to understand how proteins are distributed inside the SBA-15 structure, if and under which conditions there is aggregation, understand protein and water dynamics over time. The following list shows how each of these topics could be studied:

- **Protein Distribution**
Imaging techniques, such as Raman, X-rays and neutron imaging, are important in order to understand how proteins are distributed inside SBA-15 [3, 26]. Some of the hypothesis we stated throughout this thesis, mainly related to homogeneity and protein distribution, could be checked with imaging techniques. These techniques should also be used used to study protein stability under the ideal conditions.
- **Protein Aggregation**
Dynamic light scattering (DLS) and Small angle X-ray and neutron scattering (SAXS and SANS) measurements would be very important, since it would allow us to study size distribution of molecules, giving us insight into any possible protein aggregation [12, 67]. This way, we would be able to probe which is the best initial concentration for encapsulation, which is, the one that leads to less aggregation.
- **Protein and Water Dynamics**
Neutron spectroscopy combined with Molecular Dynamics simulations

could give us insight into adsorption dynamics and allows us to better understand how this process happens under different conditions [68].

It would be very interesting to understand if these results are reproducible. We could repeat the process described in this thesis with a few modifications. A more reliable fit would require even more data points and from the modelling point of view, different approaches to fit the data could be interesting. Based on techniques mentioned above, we would have more information on adsorption dynamics and would be able to understand which model better suits each pH condition. This way, the parameters obtained from the fittings would be more accurate and reliable [34]. It could be advantageous to, also, track the samples overtime, in order to understand if there is any change in the samples, since time might be one additional condition that we are not considering.

Bibliography

- [1] Anna M Acosta et al. *Español | Other Languages Epidemiology and Prevention of Vaccine-Preventable Diseases Epidemiology and Prevention of Vaccine-Preventable Diseases Home Diphtheria*. Tech. rep. URL: <https://www.cdc.gov/vaccines/pubs/pinkbook/dip.html>.
- [2] Andreas Burkovski. *Corynebacterium diphtheriae and related toxigenic species: Genomics, pathogenicity and applications*. Vol. 9789400776241. Springer Netherlands, Aug. 2014, pp. 1–293. ISBN: 9789400776241. DOI: 10.1007/978-94-007-7624-1.
- [3] Martin Kjærulf Rasmussen et al. „Assessing the efficiency of SBA-15 as a nanocarrier for diphtheria anatoxin“. In: *Microporous and Mesoporous Materials* 312 (Jan. 2021). ISSN: 13871811. DOI: 10.1016/j.micromeso.2020.110763.
- [4] Husam Alsarraf et al. *Biophysical comparison of diphtheria and tetanus toxins with the formaldehyde-detoxified toxoids, the main components of diphtheria and tetanus vaccines*. Nov. 2017. DOI: 10.1080/21505594.2017.1321726.
- [5] Sunita Awate, Lorne A. Babiuk, and George Mutwiri. *Mechanisms of action of adjuvants*. 2013. DOI: 10.3389/fimmu.2013.00114.
- [6] *Epidemiological Update Diphtheria*. Tech. rep. 2017. URL: <http://www.paho.xn--orgpaho-qja6263e/WHO,2017>.
- [7] Qing Zhu and Jay A. Berzofsky. „Oral vaccines“. In: *Gut Microbes* 4.3 (May 2013), pp. 246–252. ISSN: 1949-0976. DOI: 10.4161/gmic.24197. URL: <http://www.tandfonline.com/doi/abs/10.4161/gmic.24197>.
- [8] G L Ada. *The ideal vaccine*. Tech. rep., pp. 105–109.

- [9] Sung Hun Kang et al. *Oral vaccine delivery for intestinal immunity-biological basis, barriers, delivery system, and M cell targeting*. Aug. 2018. DOI: 10.3390/polym10090948.
- [10] Ali Azizi et al. *Enhancing oral vaccine potency by targeting intestinal M cells*. Nov. 2010. DOI: 10.1371/journal.ppat.1001147.
- [11] Karishma T. Physical properties of ordered mesoporous SBA-15 silica as immunological adjuvant Mody et al. *Mesoporous silica nanoparticles as antigen carriers and adjuvants for vaccine delivery*. June 2013. DOI: 10.1039/c3nr00357d.
- [12] Martin K. Rasmussen et al. „3D visualisation of hepatitis B vaccine in the oral delivery vehicle SBA-15“. In: *Scientific Reports* 9.1 (Dec. 2019). ISSN: 20452322. DOI: 10.1038/s41598-019-42645-5.
- [13] C. L.P. Oliveira et al. „The development of new oral vaccines using porous silica“. In: *Journal of Physics Condensed Matter* 34.26 (June 2022). ISSN: 1361648X. DOI: 10.1088/1361-648X/ac6559.
- [14] Vladimir L. Zholobenko et al. *Initial stages of SBA-15 synthesis: An overview*. Oct. 2008. DOI: 10.1016/j.cis.2008.05.003.
- [15] Reyna Ojeda-López et al. „SBA-15 materials: calcination temperature influence on textural properties and total silanol ratio“. In: *Adsorption* 21.8 (Nov. 2015), pp. 659–669. ISSN: 15728757. DOI: 10.1007/s10450-015-9716-2.
- [16] Parya Kazemzadeh et al. *Structure-Property Relationship for Different Mesoporous Silica Nanoparticles and its Drug Delivery Applications: A Review*. Mar. 2022. DOI: 10.3389/fchem.2022.823785.
- [17] Emma M. Björk. „Synthesizing and characterizing mesoporous silica SBA-15: A hands-on laboratory experiment for undergraduates using various instrumental techniques“. In: *Journal of Chemical Education* 94.1 (Jan. 2017), pp. 91–94. ISSN: 19381328. DOI: 10.1021/acs.jchemed.5b01033.
- [18] Adriano M. Basso et al. „Tunable effect of the calcination of the silanol groups of KIT-6 and SBA-15 mesoporous materials“. In: *Applied Sciences (Switzerland)* 10.3 (Feb. 2020). ISSN: 20763417. DOI: 10.3390/app10030970.

- [19] Jens Meissner et al. „Protein immobilization in surface-functionalized SBA-15: Predicting the uptake capacity from the pore structure“. In: *Journal of Physical Chemistry C* 119.5 (Feb. 2015), pp. 2438–2446. ISSN: 19327455. DOI: 10.1021/jp5096745.
- [20] Bhuvnesh Bharti et al. „Bridging interactions of proteins with silica nanoparticles: The influence of pH, ionic strength and protein concentration“. In: *Soft Matter* 10.5 (Feb. 2014), pp. 718–728. ISSN: 1744683X. DOI: 10.1039/c3sm52401a.
- [21] Lung Ching Sang, Ajayan Vinu, and Marc Olivier Coppens. „General description of the adsorption of proteins at their iso-electric point in nanoporous materials“. In: *Langmuir* 27.22 (Nov. 2011), pp. 13828–13837. ISSN: 07437463. DOI: 10.1021/la202907f.
- [22] Chemistry LibreTexts. *pH Chemistry LibreTexts*. URL: [https://chem.libretexts.org/Bookshelves/Introductory_Chemistry/Chemistry_for_Allied_Health_\(Soul\)/08%3A_Properties_of_Solutions/8.06%3A_The_pH_Concept](https://chem.libretexts.org/Bookshelves/Introductory_Chemistry/Chemistry_for_Allied_Health_(Soul)/08%3A_Properties_of_Solutions/8.06%3A_The_pH_Concept).
- [23] Manuel E. Sastre de Vicente. „The Concept of Ionic Strength Eighty Years after Its Introduction in Chemistry“. In: (). ISSN: 0021-9584. DOI: 10.1021/ed081p750.
- [24] Jens Meissner et al. „Characterization of protein adsorption onto silica nanoparticles: influence of pH and ionic strength“. In: *Colloid and Polymer Science* 293.11 (Nov. 2015), pp. 3381–3391. ISSN: 14351536. DOI: 10.1007/s00396-015-3754-x.
- [25] *PZC IUPAC*. URL: <https://goldbook.iupac.org/terms/view/P04704>.
- [26] Márcia Carvalho De Abreu Fantini et al. *Using crystallography tools to improve vaccine formulations*. Jan. 2022. DOI: 10.1107/S205225252101071X.
- [27] Patrizia Ferraboschi, Samuele Ciceri, and Paride Grisenti. *Applications of lysozyme, an innate immune defense factor, as an alternative antibiotic*. Dec. 2021. DOI: 10.3390/antibiotics10121534.
- [28] H I R O Y U K I Shirahama, Johannes Lyklema, and Willem N O R D E. *Comparative Protein Adsorption in Model Systems*. Tech. rep. 1990.
- [29] *Diphtheria toxin Structure PDB*. URL: <https://www.rcsb.org/structure/1f01>.
- [30] *Lysozyme Structure PDB*. URL: <https://www.rcsb.org/structure/1DPX>.

- [31] Jacquie. *Chapter 1: UV-Visible & Fluorescence Spectroscopy*. Tech. rep.
- [32] Thermo Scientific NanoDrop Spectrophotometers Protein A280 Protein A280. Tech. rep. 2010.
- [33] Éder Cláudio Lima et al. „Adsorption: Fundamental aspects and applications of adsorption for effluent treatment“. In: *Green Technologies for the Defluoridation of Water*. Elsevier, Jan. 2021, pp. 41–88. ISBN: 9780323857680. DOI: 10.1016/B978-0-323-85768-0.00004-X.
- [34] Robert A. Latour. „The Langmuir isotherm: A commonly applied but misleading approach for the analysis of protein adsorption behavior“. In: *Journal of Biomedical Materials Research - Part A* 103.3 (Mar. 2015), pp. 949–958. ISSN: 15524965. DOI: 10.1002/jbm.a.35235.
- [35] „Thermal_methods_of_analysis_Wendlandt_We“. In: ().
- [36] P. R.A.F. Garcia et al. „Protein encapsulation in SBA-15 with expanded pores“. In: *Microporous and Mesoporous Materials* 235 (Nov. 2016), pp. 59–68. ISSN: 13871811. DOI: 10.1016/j.micromeso.2016.07.033.
- [37] Merck. *PBS P4417 Sigma Aldrich*. URL: <https://www.sigmaaldrich.com/DK/en/product/sigma/p4417>.
- [38] Simon Lind et al. *Using model proteins to predict incorporation behavior into SBA-15 mesoporous silica: A step towards oral vaccine development*. Tech. rep.
- [39] Implen. *UV-Vis spectrometers*. URL: <https://www.implen.de/uv-vis-spectrophotometer/>.
- [40] Agilent Technologies. *Peptide and Amino Acid Quantification Using UV Fluorescence in Synergy HT Multi-Mode Microplate Reader*. Tech. rep. 2006. URL: www.biotek.com.
- [41] Jim Clark LibreTexts Chemistry. *The Beer-Lambert Law LibreTexts*. URL: [https://chem.libretexts.org/Bookshelves/Physical_and_Theoretical_Chemistry_Textbook_Maps/Supplemental_Modules_\(Physical_and_Theoretical_Chemistry\)/Spectroscopy/Electronic_Spectroscopy/Electronic_Spectroscopy_Basics/The_Beer-Lambert_Law#title](https://chem.libretexts.org/Bookshelves/Physical_and_Theoretical_Chemistry_Textbook_Maps/Supplemental_Modules_(Physical_and_Theoretical_Chemistry)/Spectroscopy/Electronic_Spectroscopy/Electronic_Spectroscopy_Basics/The_Beer-Lambert_Law#title).
- [42] Saeid Azizian, Setareh Eris, and Lee D. Wilson. „Re-evaluation of the century-old Langmuir isotherm for modeling adsorption phenomena in solution“. In: *Chemical Physics* 513 (Sept. 2018), pp. 99–104. ISSN: 03010104. DOI: 10.1016/j.chemphys.2018.06.022.

- [43] *Curve_Fit online Documentation*. URL: https://docs.scipy.org/doc/scipy/reference/generated/scipy.optimize.curve_fit.html.
- [44] C. J. Spencer, C. Yakymchuk, and M. Ghaznavi. „Visualising data distributions with kernel density estimation and reduced chi-squared statistic“. In: *Geoscience Frontiers* 8.6 (Nov. 2017), pp. 1247–1252. ISSN: 16749871. DOI: 10.1016/j.gsf.2017.05.002.
- [45] PerkinElmer Inc. *Thermogravimetric Analysis (TGA) TGA 8000 TGA 4000 STA 6000 / STA 8000 The Thermogravimetric Instrument Family*. Tech. rep.
- [46] *THERMAL ANALYSIS OF POLYMERS - Fundamentals and Applications*. Tech. rep.
- [47] Nooshin Saadatkhah et al. *Experimental methods in chemical engineering: Thermogravimetric analysis—TGA*. Jan. 2020. DOI: 10.1002/cjce.23673.
- [48] Steven A. Yamada et al. „Effects of pore size on water dynamics in mesoporous silica“. In: *Journal of Chemical Physics* 152.15 (Apr. 2020). ISSN: 00219606. DOI: 10.1063/1.5145326.
- [49] Yoshiyuki Yokogawa et al. „Kinetic modelling of cytochrome c adsorption on SBA-15“. In: *Bio-Medical Materials and Engineering* 28.1 (2017), pp. 37–46. ISSN: 18783619. DOI: 10.3233/BME-171654.
- [50] Yaakov Levy and José N Onuchic. *Water and proteins: A love-hate relationship*. Tech. rep. 2004. URL: www.pnas.org/cgi/doi/10.1073/pnas.0400157101.
- [51] Marie Claire Bellissent-Funel et al. *Water Determines the Structure and Dynamics of Proteins*. July 2016. DOI: 10.1021/acs.chemrev.5b00664.
- [52] Jürgen H Gross. *Mass Spectrometry*. Tech. rep.
- [53] Rob ten Haaf Bronkhorst. *Mass Spectrometry and Mass Flow Control; A closer ion them*. Aug. 2022. URL: <https://www.bronkhorst.com/int/blog-1/mass-spectrometry-and-mass-flow-control-a-closer-ion-them/>.
- [54] *Mass Specrometer*. URL: <http://hyperphysics.phy-astr.gsu.edu/hbase/magnetic/maspec.html>.
- [55] „ThermalDecompositionofOxalate“. In: ()

- [56] Libre Texts Chemistry. *Infrared Spectroscopy*. Apr. 2022. URL: [https://chem.libretexts.org/Bookshelves/Physical_and_Theoretical_Chemistry_Textbook_Maps/Supplemental_Modules_\(Physical_and_Theoretical_Chemistry\)/Spectroscopy/Vibrational_Spectroscopy/Infrared_Spectroscopy](https://chem.libretexts.org/Bookshelves/Physical_and_Theoretical_Chemistry_Textbook_Maps/Supplemental_Modules_(Physical_and_Theoretical_Chemistry)/Spectroscopy/Vibrational_Spectroscopy/Infrared_Spectroscopy).
- [57] Tom Tyner and James Francis. *ACS Reagent Chemicals*. Washington, DC: American Chemical Society, Jan. 2017. ISBN: 9780841230460. DOI: 10.1021/acsreagents. URL: <https://pubs.acs.org/doi/book/10.1021/acsreagents>.
- [58] Oluwatobi Samuel Oluwafemi et al. „Characterization techniques for ternary I–III–VI quantum dots“. In: *Ternary Quantum Dots*. Elsevier, 2021, pp. 117–135. DOI: 10.1016/b978-0-12-818303-8.00007-1.
- [59] Paul. Gabbott. *Principles and applications of thermal analysis*. Blackwell Pub, 2008, p. 464. ISBN: 9781405131711.
- [60] „Infrared Spectrum of Carbon Dioxide“. In: (). URL: <https://webbook.nist.gov/cgi/cbook.cgi?ID=C124389&Units=SI&Type=IR-SPEC&Index=0#IR-SPEC>.
- [61] NIST. *water Infrared Spectrum*. URL: <https://webbook.nist.gov/cgi/cbook.cgi?ID=C7732185&Type=IR-SPEC&Index=0#IR-SPEC>.
- [62] F. Bérubé and S. Kaliaguine. „Calcination and thermal degradation mechanisms of triblock copolymer template in SBA-15 materials“. In: *Microporous and Mesoporous Materials* 115.3 (Nov. 2008), pp. 469–479. ISSN: 13871811. DOI: 10.1016/j.micromeso.2008.02.028.
- [63] Daniela Steri, Maura Monduzzi, and Andrea Salis. „Ionic strength affects lysozyme adsorption and release from SBA-15 mesoporous silica“. In: *Microporous and Mesoporous Materials* 170 (2013), pp. 164–172. ISSN: 13871811. DOI: 10.1016/j.micromeso.2012.12.002.
- [64] Martin K. Rasmussen et al. „Dynamics of encapsulated hepatitis B surface antigen: A combined neutron spectroscopy and thermo-analysis study“. In: *European Physical Journal: Special Topics* 227.17 (Mar. 2019), pp. 2393–2399. ISSN: 19516401. DOI: 10.1140/epjst/e2019-700103-x.
- [65] Masaru Tanaka, Shigeaki Morita, and Tomohiro Hayashi. „Role of interfacial water in determining the interactions of proteins and cells with hydrated materials“. In: *Colloids and Surfaces B: Biointerfaces* 198 (Feb. 2021). ISSN: 18734367. DOI: 10.1016/j.colsurfb.2020.111449.

- [66] Andrea Salis, Mani S. Bhattacharyya, and Maura Monduzzi. „Specific Ion Effects on Adsorption of Lysozyme on Functionalized SBA-15 Mesoporous Silica“. In: *Journal of Physical Chemistry B* 114.23 (June 2010), pp. 7996–8001. ISSN: 15205207. DOI: 10.1021/jp102427h.
- [67] Danilo W. Losito et al. „Biocomposites based on SBA-15 and papain: Characterization, enzymatic activity and cytotoxicity evaluation“. In: *Microporous and Mesoporous Materials* 325 (Oct. 2021). ISSN: 13871811. DOI: 10.1016/j.micromeso.2021.111316.
- [68] Arantxa Arbe, Fernando Alvarez, and Juan Colmenero. *Insight into the structure and dynamics of polymers by neutron scattering combined with atomistic molecular dynamics simulations*. Dec. 2020. DOI: 10.3390/polym12123067.

Appendix

6.1 Appendix A

All the buffer recipes were taken from <https://www.liverpool.ac.uk/pfg/Tools/BufferCalc/Buffer.html>. The website provides a recipe and an alternative recipe; we used the alternative recipe for all of them.

- Phosphate Buffer ($pK_{a1} = 2.15$), pH = 2.9, Ionic Strength = 150mM

Dissolve 0.49 g of Phosphoric acid (Mr = 98) in approximately 450 ml of pure water.

Add 4.132 g of NaCl.

Titrate to pH 2.9 at the lab temperature of 23 °C with monovalent strong base or acid as needed.

Make up volume to 500 ml with pure water.

- Acetate Buffer ($pK_a = 4.76$), pH = 5.6, Ionic Strength = 150mM

Dissolve 0.30025 g of Acetic acid (Mr = 60.05) in approximately 450 ml of pure water.

Add 4.127 g NaCl.

Titrate to pH 5.6 at the lab temperature of 23 °C with monovalent strong base or acid as needed.

Make up volume to 500 ml with pure water.

- Phosphate Buffer ($pK_{a2} = 7.2$), pH = 7.4, Ionic Strength = 150mM

Dissolve 0.6 g of e.g. NaH_2PO_4 (Mr = 120) in approximately 450 ml of pure water.

Add 3.635 g NaCl.

Titrate to pH 7.4 at the lab temperature of 23 °C with monovalent strong base or acid as needed.

Make up volume to 500 ml with pure water.

- CHES Buffer ($pK_a = 9.41$), pH = 9.1, Ionic Strength = 150mM

Dissolve 1.0365 g of CHES free acid (Mr = 207.3) in approximately 450 ml of pure water.

Add 4.28 g NaCl.

Titrate to pH 9.09 at the lab temperature of 23 °C with monovalent strong base or acid as needed.

Make up volume to 500 ml with pure water.

In order to mix the buffer component with NaCl, we used a magnetic stirrer. For titration process, we used 0.04mg/mL hydrochloric acid and sodium hydroxide solutions, as a strong acid and base respectively: using a pH meter, we measured the solution's pH and added the necessary acid or base until we get the desired pH for each buffer.

- PBS Buffer

We prepared this buffer by dissolving one tablet of PBS, sourced from Sigma-Aldrich. in 200 mL of deionized water.

6.2 Appendix B

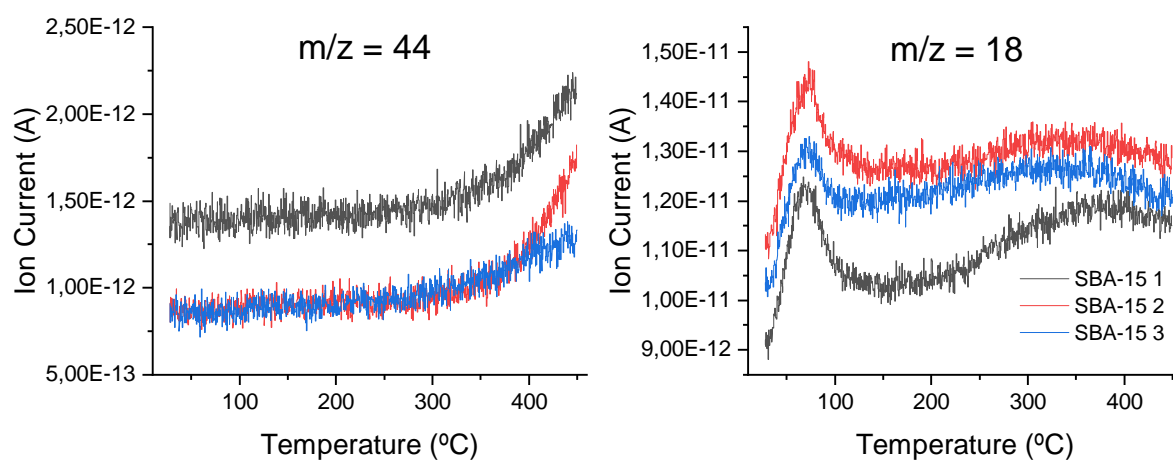


Figure 6.1: Left: MS at $m/z = 44$. Right: MS at $m/z = 18$ for SBA-15 1 (black), 2 (red) and 3 (blue).

6.3 Appendix C

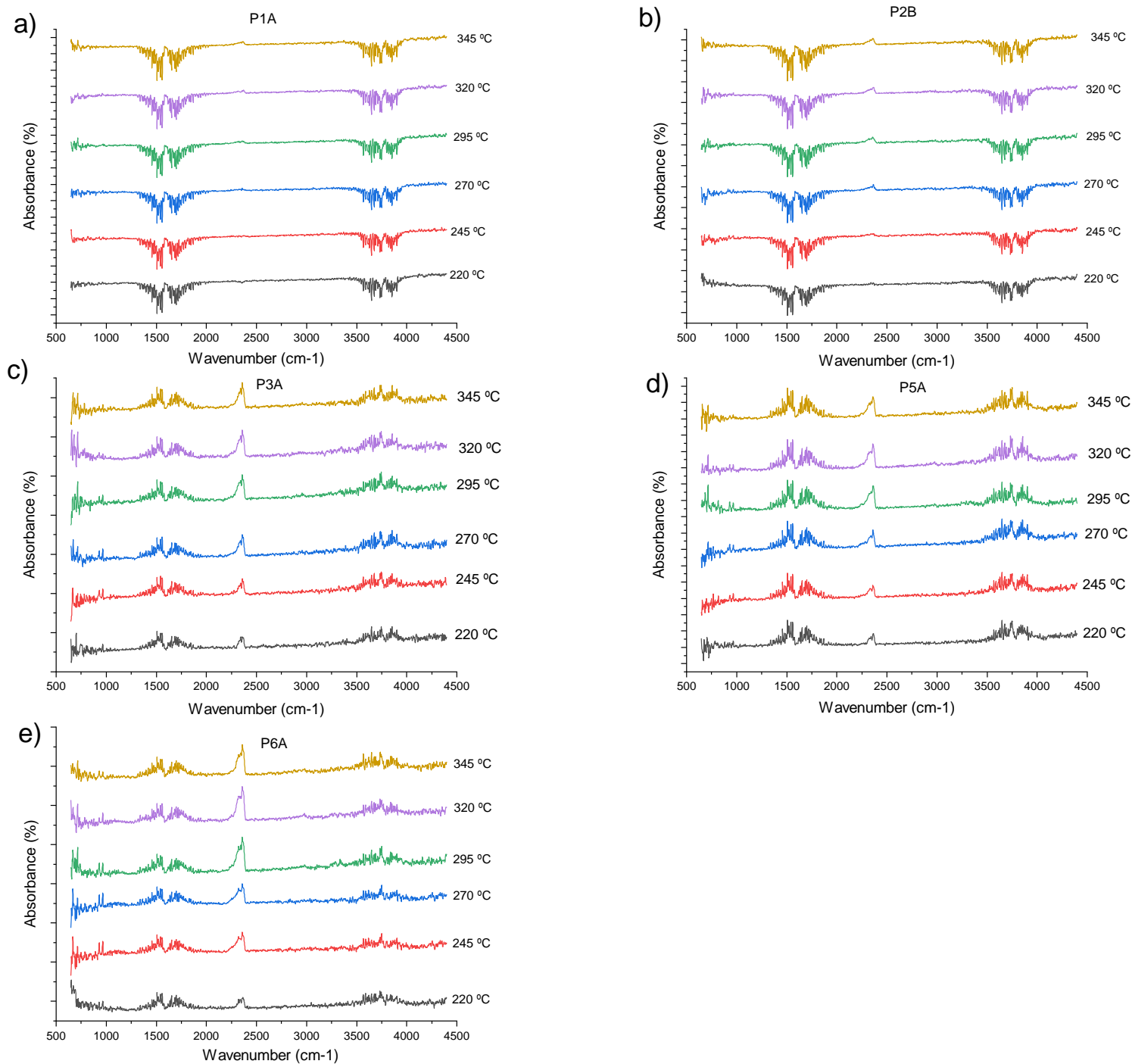


Figure 6.2: FTIR of Lysozyme samples: a)P1A , b) P2B c)P3A d)P5A e)P6A.

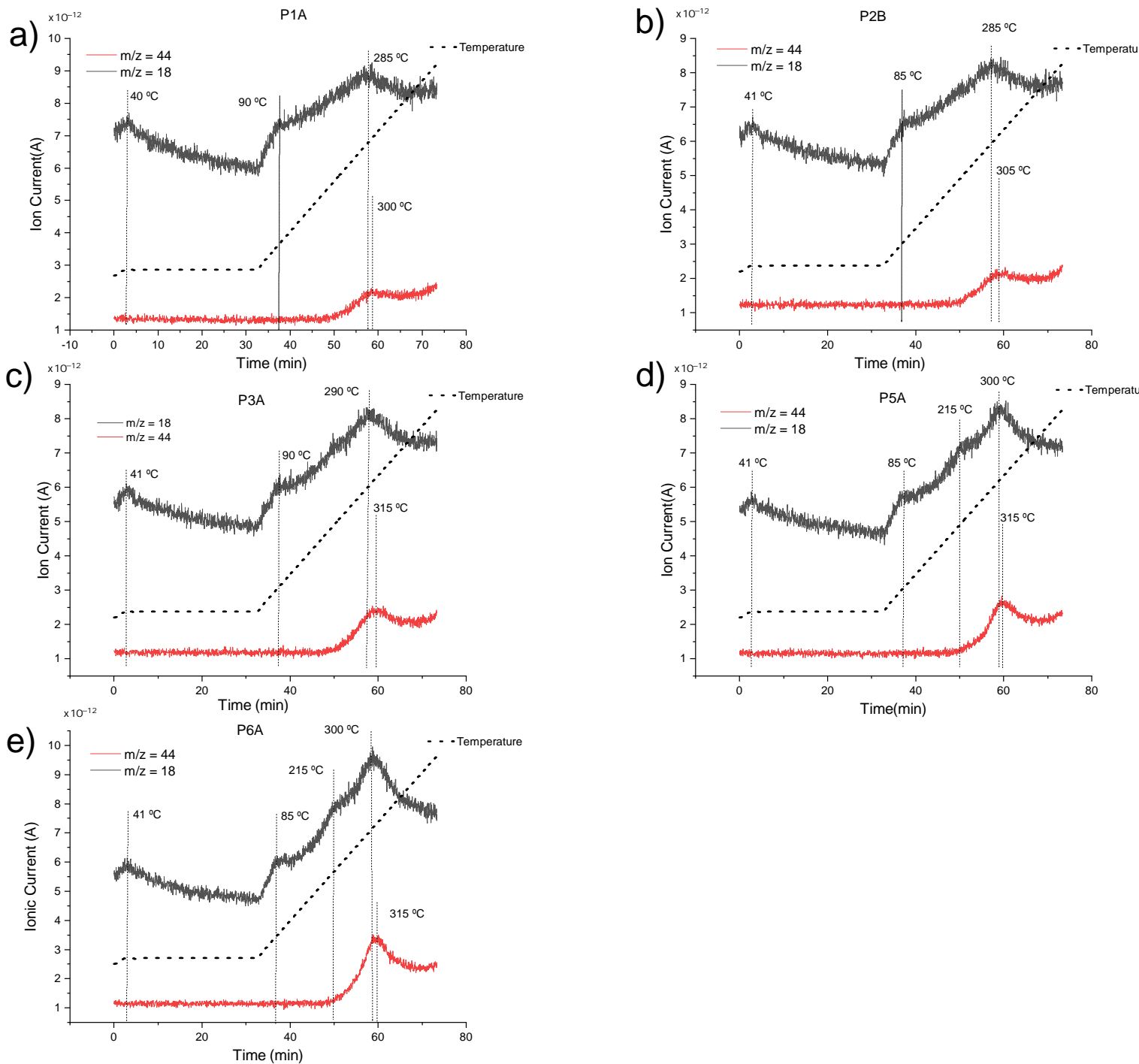


Figure 6.3: MS profile of Lysozyme samples at $m/z = 18$ (black) and $m/z = 44$ (red): a)P1A , b) P2B c)P3A d)P5A e)P6A. The temperature line shows where the isochrom set for these measurements finished.

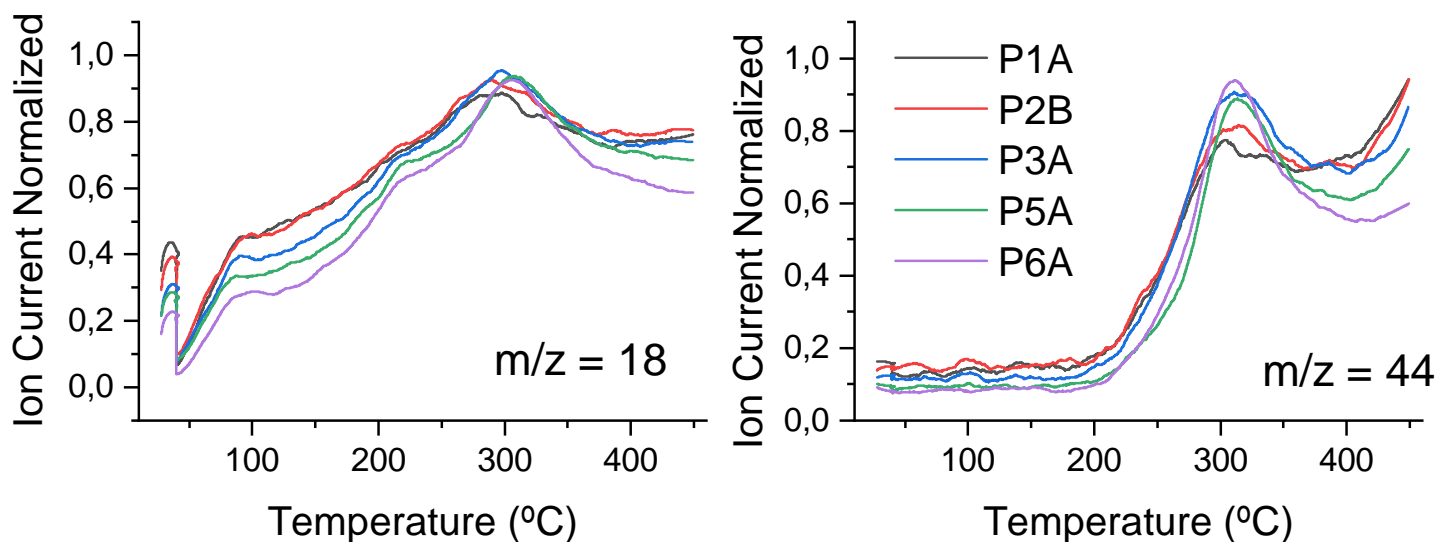


Figure 6.4: Left: MS at $m/z = 18$ normalized and smoothed. Right: MS at $m/z = 44$ normalized and smoothed. Black curve corresponds to sample P1A, red to P2B, blue to P3A, green P5A and purple to P6A.

6.4 Appendix D

Tables 6.1 and 6.2 show the experimental values and errors associated to each Lys sample prepared: mass of SBA-15 (m_{SBA-15} , initial and final concentration (c_i and c_f) and protein mass ($m_{protein}$) for first and second set of samples. As mentioned before, initial and final concentration correspond to the measured concentration before and after adding SBA-15 to the sample mix.

Error on m_{SBA15} only considers the balance accuracy. c_i and c_f correspond to the mean value of 3 measurements and the errors are calculated considering statistical errors and the instruments' accuracy:

$$\sqrt{\frac{\sum (x - \bar{x})^2}{n(n-1)} + \sigma_{accur}^2} \quad (6.1)$$

The UV-Vis spectrometer and the balance have an estimated accuracy of 0.05 mg/mL and 0.5 mg. Therefore 0.05 mg/mL and 0.5 mg are the σ_{accur} associated to concentration (initial and final) and mass, respectively. The volume of

Table 6.1: Information on mass of SBA-15, initial and final concentration of first data set of lysozyme incorporated into SBA-15 and PBS buffer.

sample	m_{SBA15} (mg)	c_i (mg/ml)	c_f (mg/mL)	$m_{protein}$ (mg)
P1A	9.5 ± 0.5	1.67 ± 0.05	0.02 ± 0.05	1.65 ± 0.07
P2A	9.7 ± 0.5	2.46 ± 0.05	0.04 ± 0.05	2.42 ± 0.07
P3A	9.5 ± 0.5	2.8 ± 0.2	0.14 ± 0.05	2.7 ± 0.3
P4A	9.4 ± 0.5	2.84 ± 0.02	0.10 ± 0.05	2.7 ± 0.1
P5A	9.6 ± 0.5	3.36 ± 0.09	0.16 ± 0.05	3.2 ± 0.1
P6A	10.7 ± 0.5	4.84 ± 0.08	0.48 ± 0.05	4.4 ± 0.1
P7A	10 ± 0.5	5.65 ± 0.09	1.57 ± 0.05	4.1 ± 0.1
P8A	10.1 ± 0.5	6.3 ± 0.1	1.39 ± 0.07	4.9 ± 0.1
P9A	10.7 ± 0.5	9.4 ± 0.3	3.4 ± 0.3	6.1 ± 0.4
P10A	10.5 ± 0.5	10.8 ± 0.2	5.83 ± 0.09	4.5 ± 0.2

Table 6.2: Information on mass of SBA-15, initial and final concentration of second data set samples of lysozyme incorporated into SBA-15 and PBS buffer.

sample #	m_{SBA15} (mg)	c_i (mg/ml)	c_f (mg/mL)	$m_{protein}$ (mg)
P1B	9.9 ± 0.5	1.5 ± 0.2	0.02 ± 0.05	1.5 ± 0.2
P2B	10.3 ± 0.5	2.2 ± 0.1	0.04 ± 0.06	2.1 ± 0.1
P3B	13.0 ± 0.5	2.23 ± 0.07	0.02 ± 0.05	2.21 ± 0.09
P4B	9.5 ± 0.5	3.31 ± 0.05	0.14 ± 0.05	3.16 ± 0.07
P5B	10.8 ± 0.5	3.5 ± 0.2	0.12 ± 0.05	3.4 ± 0.2
P6B	10.3 ± 0.5	4.40 ± 0.09	0.71 ± 0.05	3.7 ± 0.1
P7B	10.1 ± 0.5	6.1 ± 0.2	1.74 ± 0.07	4.4 ± 0.2
P8B	10.4 ± 0.5	7.7 ± 0.3	2.4 ± 0.2	5.4 ± 0.3
P9B	10.4 ± 0.5	9.9 ± 0.2	4.84 ± 0.07	5.0 ± 0.3
P10B	10.5 ± 0.5	10.8 ± 0.1	6.0 ± 0.4	4.8 ± 0.4

protein dispersion added to the samples is constant (1 ml) and there is no associated error, since the errors on the micropipettes are set to 0.

The error on on the protein intake capacity (equation 1) was calculated with error propagation, including the errors from m_{SBA-15} , c_i and c_f :

$$\sigma_{adsorp} = adsorp \cdot \sqrt{\frac{V^2 \cdot (\sigma_{c_i}^2 + \sigma_{c_f}^2)}{m_{prot}^2} + \left(\frac{\sigma_{m_{SBA}}}{m_{SBA}}\right)^2} \quad (6.2)$$

6.5 Appendix E

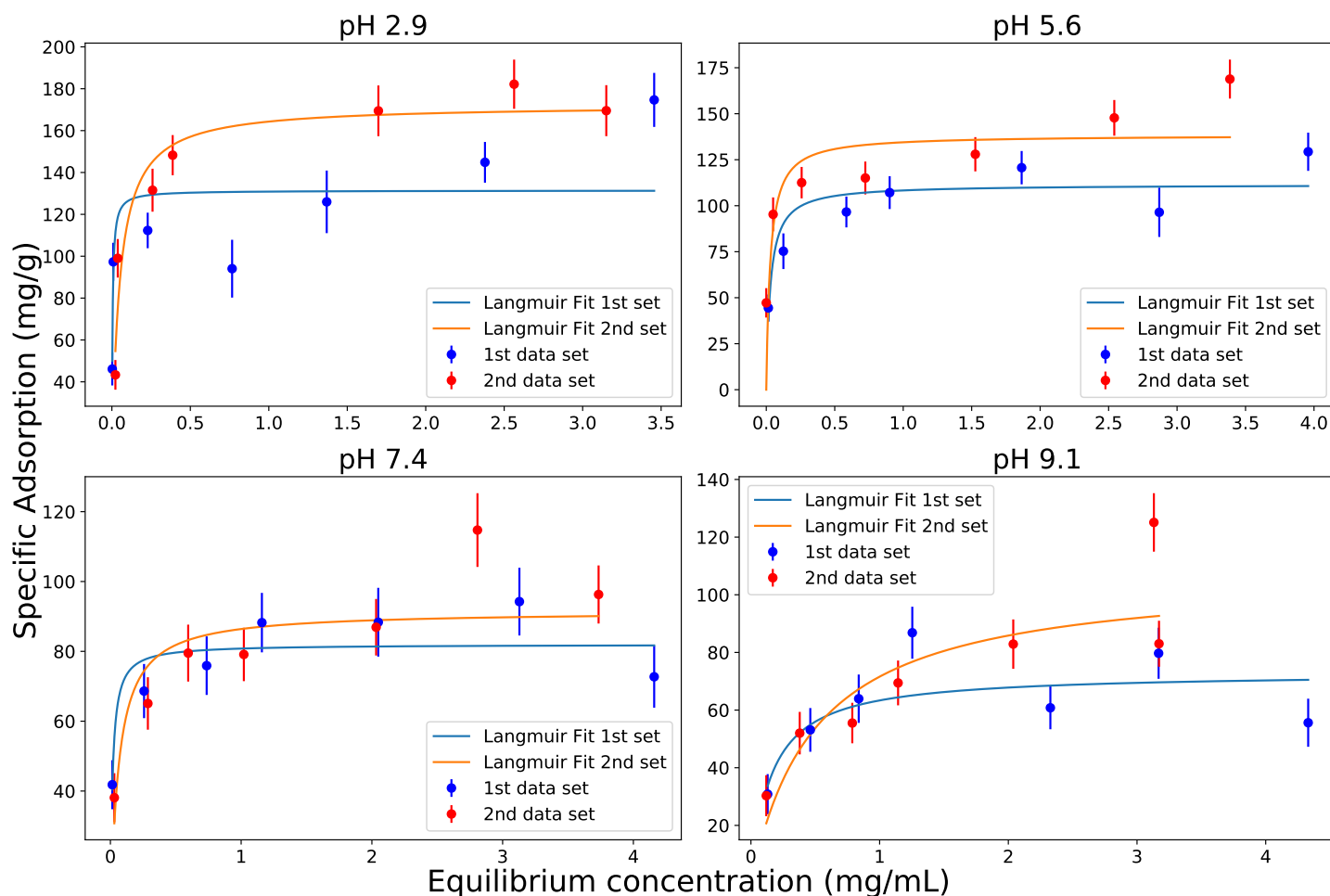


Figure 6.5: Isotherm of DT into SBA-15 at different pH for first and second set (red points) of samples and respective Langmuir fits for : pH 2.9 (upper left), pH 5.6 (upper right), pH 7.4 (bottom left) and pH 9.1 (bottom right). Points represents datapoints (blue for first and red for second data set), vertical line represents the error on the y-axis and solid lines correspond to the Langmuir fit (blue for first and yellow for second data sets).

6.6 Appendix F

Tables (6.3,6.4, 6.5 and 6.6) show the mass of SBA-15 (m_{SBA-15}), initial and final concentration (c_i and c_f) and protein intake ($m_{protein}$) for DT adsorption

into SBA-15, for pH 2.9, 5.6, 7.4 and 9.1, respectively. Errors were calculated exactly the same as for Lys into SBA-15 (Appendix C).

- pH 2.9

Table 6.3: Information on mass of SBA-15, initial and final concentration for DT incorporation into SBA-15 at pH 2.9.

sample #	m_{SBA} (mg)	c_i (mg/mL)	c_f (mg/mL)	m_{prot} (mg)
1	9.6 ± 0.5	0.45 ± 0.05	0.003 ± 0.050	0.44 ± 0.07
2	9.5 ± 0.5	0.93 ± 0.05	0.01 ± 0.05	0.93 ± 0.07
3	10.9 ± 0.5	1.45 ± 0.05	0.23 ± 0.05	1.22 ± 0.07
4	10.7 ± 0.5	1.8 ± 0.1	0.77 ± 0.05	1.0 ± 0.1
5	10.3 ± 0.5	2.7 ± 0.1	1.37 ± 0.06	1.3 ± 0.1
6	10.7 ± 0.5	3.93 ± 0.05	2.38 ± 0.05	1.55 ± 0.07
7	9.9 ± 0.5	5.19 ± 0.08	3.46 ± 0.05	1.7 ± 0.1

- pH 5.6

Table 6.4: Information on mass of SBA-15, initial and final concentration for DT incorporation into SBA-15 at pH 5.6.

sample #	m_{SBA} (mg)	c_i (mg/mL)	c_f (mg/mL)	m_{prot} (mg)
1	10.3 ± 0.5	0.47 ± 0.05	0.02 ± 0.05	0.46 ± 0.07
2	9.4 ± 0.5	0.83 ± 0.06	0.13 ± 0.05	0.71 ± 0.08
3	10.3 ± 0.5	1.58 ± 0.05	0.59 ± 0.05	1.00 ± 0.07
4	10.0 ± 0.5	1.97 ± 0.05	0.90 ± 0.05	1.07 ± 0.07
5	10.4 ± 0.5	3.12 ± 0.05	1.87 ± 0.05	1.25 ± 0.07
6	10.5 ± 0.5	3.9 ± 0.1	2.87 ± 0.05	1.0 ± 0.1
7	10.4 ± 0.5	5.30 ± 0.07	3.96 ± 0.05	1.34 ± 0.08

- pH 7.4

Table 6.5: Information on mass of SBA-15, initial and final concentration for DT incorporation into SBA-15 at pH 7.4.

sample #	m_{SBA} (mg)	c_i (mg/mL)	c_f (mg/mL)	m_{prot} (mg)
1	10.6 ± 0.5	0.46 ± 0.05	0.01 ± 0.05	0.44 ± 0.07
2	10.2 ± 0.5	0.96 ± 0.05	0.26 ± 0.05	0.70 ± 0.07
3	9.7 ± 0.5	1.48 ± 0.05	0.74 ± 0.05	0.74 ± 0.07
4	10.3 ± 0.5	2.07 ± 0.06	1.16 ± 0.05	0.91 ± 0.07
5	10.4 ± 0.5	2.97 ± 0.08	2.05 ± 0.05	0.92 ± 0.09
6	9.7 ± 0.5	4.04 ± 0.06	3.13 ± 0.05	0.91 ± 0.08
7	9.5 ± 0.5	4.85 ± 0.05	4.16 ± 0.05	0.69 ± 0.07

- pH 9.1

Table 6.6: Information on mass of SBA-15, initial and final concentration for DT incorporation into SBA-15 at pH 9.1.

sample #	m_{SBA} (mg)	c_i (mg/mL)	c_f (mg/mL)	m_{prot} (mg)
1	10.7 ± 0.5	0.46 ± 0.05	0.13 ± 0.05	0.33 ± 0.07
2	10.0 ± 0.5	1.00 ± 0.05	0.46 ± 0.05	0.53 ± 0.07
3	9.5 ± 0.5	1.45 ± 0.05	0.84 ± 0.05	0.61 ± 0.07
4	9.4 ± 0.5	2.07 ± 0.05	1.25 ± 0.05	0.82 ± 0.07
5	10.5 ± 0.5	2.97 ± 0.05	2.33 ± 0.05	0.64 ± 0.07
6	9.5 ± 0.5	3.93 ± 0.05	3.17 ± 0.05	0.76 ± 0.07
7	9.8 ± 0.5	4.88 ± 0.05	4.33 ± 0.06	0.54 ± 0.08

6.7 Appendix G

Table 6.7: Information on mass of samples used for checking SBA-15 reproducibility: SBA-15 1, 2 and 3.

Sample	Mass (mg)
SBA-15 1	4.4
SBA-15 2	4.1
SBA-15 3	4.0

Table 6.8: Information on mass of samples used for checking reproducibility of DT control samples for each pH: CA450, CB450 and CB1050.

pH	Sample	Mass (mg)
2.9	CA450	2
	CB450	1.9
	CB1050	2.4
5.6	CA450	2.8
	CB450	2.7
	CB1050	2.8
7.4	CA450	2.8
	CB450	2.9
	CB1050	3.1
9.1	CA450	2.7
	CB450	2.1
	CB1050	2.8

Table 6.9: Information on mass of samples used for comparison of DT first and second set of samples: P2 and P4.

pH	Sample	A/B	Mass (mg)
2.9	P2	A	2.6
		B	2.3
	P4	A	2.2
		B	2.2
5.6	P2	A	2.5
		B	2.7
	P4	A	2.8
		B	2.5
7.4	P2	A	2.7
		B	2.6
	P4	A	2.9
		B	2.5
9.1	P2	A	3.2
		B	2.8
	P4	A	3.6
		B	2.9